UNIVERSIDADE FEDERAL DE MINAS GERAIS
Escola de Engenharia
Programa de Pós-Graduação em Engenharia Metalúrgica, Materiais e de Minas

Bruna Nepomuceno e Vidigal

INFLUENCE OF PIPE SURFACE GRINDING ON FATIGUE LIFE OF SEAMLESS LINE PIPE API X65QS/QO PSL2 OFFSHORE

Belo Horizonte
2024

Bruna Nepomuceno e Vidigal

INFLUÊNCIA DO ESMERILHAMENTO NA SUPERFÍCIE DO TUBO NA VIDA EM FADIGA DE TUBOS DE AÇO SEM COSTURA X65QS/QO OFFSHORE

Dissertação apresentada ao Programa de Pós-Graduação em Engenharia Metalúrgica, de Materiais e de Minas da Escola de Engenharia da Universidade Federal de Minas Gerais, como requisito parcial à obtenção do título de mestre em Engenharia Metalúrgica, Materiais e de Minas.

Área de Concentração: Metalurgia Física.

Orientador: Professor Pedro Henrique Rodrigues Pereira

Coorientador: Vicente Braz da Trindade Filho

Belo Horizonte
2024

Vidigal, Bruna Nepomuceno e.
V653i Influência do esmerilhamento na superfície do tubo na vida em fadiga de tubos de aço sem costura X65QS/QO offshore [recurso eletrônico] / Bruna Nepomuceno e Vidigal. - 2024.
1 recurso online (78 f.: il., color.) : pdf.

Orientador: Pedro Henrique Rodrigues Pereira.
Coorientador: Vicente Braz da Trindade Filho.

Dissertação (mestrado) - Universidade Federal de Minas Gerais, Escola de Engenharia.

Inclui bibliografia.

1. Engenharia metalúrgica - Teses. 2. Metalurgia física - Teses. 3. Aço - Fadiga - Teses. 4. Metais - Têmpera - Teses. I. Pereira, Pedro Henrique Rodrigues. II. Trindade Filho, Vicente Braz da. III. Universidade Federal de Minas Gerais. Escola de Engenharia. IV. Título.

CDU: 669(043)

Ficha catalográfica elaborada pelo bibliotecário Reginaldo César Vital dos Santos CRB/6 2165
Biblioteca Prof. Mário Werneck, Escola de Engenharia da UFMG

UNIVERSIDADE FEDERAL DE MINAS GERAIS
ESCOLA DE ENGENHARIA
Programa de Pós-Graduação em Engenharia Metalúrgica, Materiais e de Minas

A dissertação intitulada **"Influence of Pipe Surface Repair on Fatigue Life of Seamless Line Pipe Api X65qs Psl2 Offshore"**, área de concentração: Metalurgia Física e de Transformação, apresentada pela candidata **Bruna Nepomuceno e Vidigal**, para obtenção do grau de Mestre em Engenharia Metalúrgica, Materiais e de Minas, foi aprovada pela comissão examinadora constituída pelos seguintes membros:

Dr. Pedro Henrique Rodrigues Pereira
Orientador (UFMG)

Dr. Vicente Braz Trindade
(VSB)

Dra. Berenice Mendonça Gonzalez
(UFMG)

Dr. Júlio Márcio Silveira e Silva
(V&M do Brasil)

Coordenador do Programa de Pós-Graduação em Engenharia Metalúrgica, Materiais e de Minas/UFMG

Belo Horizonte, 09 de setembro de 2024

RESUMO

Experimentos foram conduzidos para avaliar o impacto da retificação superficial na vida útil à fadiga de tubos sem costura constituídos pelo aço API 5L X65QS. Para tal, tubos de aço produzidos sob condições equivalentes foram submetidos a ensaios de fadiga em escala real após passarem por (i) tratamento térmico de têmpera e revenimento, seguido de (ii) esmerilhamento das superfícies circunferenciais internas e (iii) externas. Observou-se que essa operação resultou em uma redução da vida útil à fadiga dos tubos sem costura. Os tubos não esmerilhados atenderam aos requisitos prescritos pela norma DNV-RP-C203, Classe B1, alcançando vida em fadiga superior a $3{,}4 \times 10^6$ ciclos para uma amplitude de tensão ($\Delta\sigma$) de 200 MPa. Em contraste, os tubos reparados internamente resistiram a aproximadamente $9{,}0 \times 10^5$ ciclos para $\Delta\sigma$ = 200 MPa, desempenho compatível com a Classe D da mesma norma. As causas subjacentes a esse comportamento foram investigadas detalhadamente, e verificou-se que o esmerilhamento não induziu alterações significativas na microestrutura do aço. A redução na vida útil à fadiga após essa operação foi atribuída à formação de pequenos entalhes nas áreas retificadas dos tubos, que atuam como concentradores de tensão, acelerando a nucleação de fissuras e, consequentemente, diminuindo a vida útil à fadiga dos tubos submetidos à operação de esmerilhamento superficial.

Palavras-chave: testes de fadiga em escala real; retificação; tubo sem costura; aplicação offshore.

ABSTRACT

Experiments were conducted to assess the effect of surface grinding on the fatigue life of API5L X65Q seamless pipes. For this purpose, steel pipes fabricated under equivalent conditions were subjected to full-scale fatigue testing after either (i) heat treatment of quench and tempering at their (ii) internal and (iii) external circumferential surfaces. The application of grinding caused a reduction in the fatigue life of the seamless tubes. The unrepaired pipes complied with the standards prescribed by DNV-RP-C203 Class B1 – Design in Air and reached fatigue endurances $>3.4 \times 10^6$ cycles for a stress amplitude ($\Delta\sigma$) of 200 MPa. Conversely, the internally ground tubes sustained down to $\sim 9.0 \times 10^5$ cycles for $\Delta\sigma = 200$ MPa which is compatible with DNV-RP-C203 Class D. The reasons underlying this behaviour were carefully investigated and it has been shown that grinding did not lead to major changes in the steel microstructures. The decrease in the fatigue life after grinding was attributed to the imprint of small steps at the repaired areas of the tubes. They act as stress concentrators and may anticipate the nucleation of cracks, ultimately, shortening the fatigue life of seamless tubes subjected to surface grinding.

Keywords: full-scale fatigue testing; grinding; seamless pipe; offshore application.

LIST OF FIGURES

LIST OF TABLES

LIST OF SIMBLES

HSLA	High-Strength and Low-Alloy
NDT	Non-Destructive Techniques
ID	Inside Diameter
OD	Outside Diameter
WT	Wall Thickness
MPI	Magnetic Particle Inspection
SEM	Scanning Electron Microscopy
$\Delta\sigma$	Stress Range (MPa)
Pi	Hydrotest pressure
SMF	Stress Modification Factor

SUMMARY

1 INTRODUCTION

1.1 English version

Offshore pipelines and risers are used to transport oil and gas over long distances. These structures are usually composed by seamless steel tubes welded on each pipe end which sustain severe loading conditions during pipe lay and operation. For this reason, High-Strength and Low-Alloy (HSLA) steels having high tensile strength and elevated fracture toughness are typically employed for these applications.

Hot rolling is done at a high temperature that can cause flaws in the material. Besides that, microstructure of the steel and inclusions can be critical factors affecting the quality of pipe surfaces which can display cracks, sweats, leaks, laminations, and other imperfections after hot rolling and het treatment. Therefore, visual inspection and/or Non-Destructive Techniques (NDT), such as ultrasonic and electromagnetic inspection shall be performed to verify pipe surfaces quality.

According to the 46th edition of the API 5L standard, seamless steel pipes for sour and offshore services may exhibit longitudinal imperfections with maximum depths of 5% of the nominal thickness of the pipe wall. Furthermore, the maximum area enclosed by each laminar imperfection may reach 500 mm^2. Imperfections with dimensions beyond these limits are classified as defects which shall be removed or repaired by grinding. In this way, the addressed area smoothly blends in with the contour of the pipe.

Offshore pipelines are under cyclic loading dynamics due to the action of waves, undersea currents, and the eventual motion of the sea ground. Also, the seamless pipes undergo straining due to periodic temperature variations and occasional impacts, in which the pipe undergoes large plastic strains. Structures undergoing number of cycles inferior to 10000 are associated with low cycle fatigue and can be found in ship parts due to loading and unloading. Structures under high cycle fatigue loading displays fatigue endurances superior to 10000 cycles. For example, it can be found as a consequence of the stress response from wave action that shows typically 5000 cycles a year, allowing the

attainment of high cycle fatigue conditions after two years. Accordingly, this load path may trigger the onset of cracks close to the repaired areas, which increase the pipes' susceptibility to fatigue failure.

Although some pipelines exhibit certain levels of defect tolerance, cracks can nucleate in pipes surfaces irregularities and propagate during pipelines operation. A catastrophic failure can occur while the structure is subject to high cyclic loads. In this context, the knowledge about the fatigue life of seamless pipes used in offshore pipelines and riser is very important, to provide information for pipeline design, materials selection during construction and predict the operational life of pipeline.

1.2 Portuguese version

Pipelines e *risers offshore* são utilizados para transportar petróleo e gás por longas distâncias. Essas estruturas são geralmente compostas por tubos de aço sem costura, soldados nas extremidades de cada tubo, que suportam condições de carregamento severas durante a instalação dos tubos e a operação. Por essa razão, aço de Alta Resistência e Baixa Liga (ARBL), com alta resistência à tração e elevada tenacidade ao fratura, é tipicamente empregado para essas aplicações.

A laminação a quente é feita a altas temperatura, o que pode causar defeitos no material. Além disso, a microestrutura do aço e as inclusões podem ser fatores críticos que afetam a qualidade das superfícies dos tubos, que podem exibir trincas, furos, descontinuidades, delaminações e outras imperfeições após a laminação a quente e o tratamento térmico. Portanto, a inspeção visual e/ou ensaios não destrutivos, como inspeção ultrassônica e eletromagnética, devem ser realizadas para verificar a qualidade das superfícies dos tubos.

De acordo com a 46ª edição do padrão API 5L, tubos de aço sem costura para aplicação em ambientes corrosivos e offshore podem apresentar imperfeições longitudinais com profundidades máximas de 5% da espessura nominal da parede do tubo. Além disso, a área máxima delimitada por cada imperfeição laminar pode alcançar 500 mm^2. Imperfeições com dimensões além desses limites são classificadas como defeitos, que devem ser removidos ou reparados por esmerilhamento. Dessa forma, a área tratada se funde suavemente com o contorno do tubo.

Os tubos offshore estão sujeitos a dinâmicas de carregamento cíclico devido à ação das ondas, correntes submarinas e ao eventual movimento do fundo do mar. Além disso, os tubos sem costura passam por deformações devido a variações periódicas de temperatura e impactos ocasionais, nos quais o tubo sofre grandes deformações plásticas. Estruturas submetidas a um número de ciclos inferior a 10.000 estão associadas à fadiga de baixo ciclo e podem ser encontradas em partes de navios devido ao carregamento e descarregamento. Estruturas sob carregamento de fadiga de alto ciclo exibem resistências

à fadiga superiores a 10.000 ciclos. Por exemplo, isso pode ser encontrado como uma consequência da resposta ao estresse da ação das ondas, que mostra tipicamente 5.000 ciclos por ano, permitindo a obtenção de condições de fadiga de alto ciclo após dois anos. Consequentemente, esse caminho de carga pode desencadear o surgimento de trincas próximas às áreas reparadas, o que aumenta a susceptibilidade dos tubos à falha por fadiga.

Embora alguns tubos apresentem certos níveis de tolerância a defeitos, trincas podem ser nucleadas em irregularidades nas superfícies dos tubos e se propagar durante a operação dos tubos. Uma falha catastrófica pode ocorrer enquanto a estrutura está sujeita a cargas cíclicas elevadas. Nesse contexto, o conhecimento sobre a vida útil à fadiga de tubos sem costura utilizados em *pipelines offshore* e *risers* é muito importante para fornecer informações para o design dos pipelines, seleção de materiais durante a construção e prever a vida operacional do pipeline.

2 OBJECTIVES

2.1 Purpose

The purpose of this study is to evaluate the effect of surface grinding on the fatigue life of X65QS/QO PSL2 seamless tubes.

2.2 Specific objectives

The specific objectives of this research are outlined as follows:

- To analyze the mechanical properties of X65QS/QO PSL2 seamless pipes, quenched and tempered, with or without grinding operation.
- To estimate the effect of the grinding process on the pipe surface and on the tribological properties.
- To evaluate the fatigue life of X65QS/QO PSL2 seamless pipes under high cycle fatigue conditions, through full-scale tests.
- To investigate the effect of grinding operations on the fatigue resistance of X65QS/QO PSL2 seamless pipes.

3 LITERATURE REVIEW

3.1 High-Strength and Low-Alloy (HSLA) steels

According to Godefroid *et al.* [1], the demand for the development and processing of materials for application in pipelines has increased over the past 30 years due to population growth and the development of petroleum dependent industries in different countries. This demand, which is more than supply, can be fulfilled either by finding out new resources or trading with other nations. Both strategies require efficient means of fuel transportation such as in continuous transportation by pipelines. They may range from few kilometers to thousand kilometers, passing through different geographical and environmental conditions. Therefore, it requires high-strength materials, such as High-Strength and Low-Alloy (HSLA) steels, to withstand different environmental conditions, considering onshore and offshore applications. [2,3]

The American Petroleum Institute (API) provides standards for pipes that are suitable for use in pipeline transportation systems in the petroleum and natural gas industries [3]. API Specification 5L, Line Pipe (API 5L) describes the requirements of chemical composition, tensile test characteristics and impact toughness for manufacturing of seamless and welded pipes with two specification levels, PSL 1 and PSL 2 [4]. Steel grades PSL1 do not have a threshold specified for carbon equivalent (CE) and only have minimum limits for yield strength and tensile strength. PSL2 grades have mandatory requirements for CE and notch toughness, in addition to the minimum and maximum limit for yield strength and tensile strength [5].

Steels are primarily classified in standard API 5L [5], according to material's yield strength which is a fundamental feature and defined as the maximum stress the material can experience without failure [4]. Identification is usually done based on an alphanumeric system where the two-digit number following the "X" indicates the minimum yield strength (in ksi) of pipe produced to this grade (e.g., X42, X56, X70). Some grades like Grades A and B are the exceptions; these do not refer to the yield strength but like all other grades, they also have specified minimum yield strength

(SMYS). Table 3.1 lists the details of various grades of steel according to API 5L [5], and the required minimum tensile and yield strength of materials.

Table 3.1 - Properties of Steels used in Line Pipe.[5]

Grade	Minimum Yield Strength MPa (psi)	Minimum Tensile Strength MPa (psi)
B	245 (35,500)	415 (60,200)
X42	290 (42,100)	415 (60,200)
X46	320 (46,400)	435 (63,100)
X52	360 (52,200)	460 (66,700)
X56	390 (56,600)	490 (71,100)
X60	415 (60,200)	520 (75,400)
X65	450 (65,300)	535 (77,600)
X70	485 (70,300)	570 (82,700)

Line Pipe steels usually exhibit very fine alloying practices classified as micro-alloying to produce high-strength materials with good weldability and low crack sensitivity coefficient. This includes a maximum weight fraction of carbon of 0.18% for seamless pipes and 0.12% for welded pipes [4,6]. The main alloying elements used HSLA steels are Nb, V, and Ti; however, others alloying elements such as Cr, Ni, Mo, and Cu are sometimes used to enhance fracture toughness, corrosion resistance and promote the development of bainite [7,8]. The effects of microalloying elements are summarized in Table 3.2.

Table 3.2 - Main effect of micro alloyed elements in HSLA steels.[7]

Element	wt.%	Effect
C	< 0.25	Strengthener
Mn	0.5 - 2.0	Retards the austenite decomposition during accelerated cooling Decrease ductile to brittle transition temperature Strong sulfide former
Si	0.1 - 0.5	Deoxidizer in molten steel Solid solution strengthener
Al	< 0.02	Deoxidizer Limits grain growths as aluminum nitride
Nb	0.02- 0.06	Very strong ferrite strengthener as niobium carbides/nitrides Delays austenite-ferrite transformation
Ti	< 0.06	Austenite grain control by titanium nitrides Strong ferrite strengthener
V	< 0.10	Strong ferrite strengthener by vanadium carbonitrides
Zr	0.002 - 0.05	Austenite grain size control Strong sulfide former
Nb	< 0.012	Strong former of nitrides and carbonitrides with micro alloyed elements
Mo	< 0.3	Promotes bainites formation Ferrite strengthener
Ni	< 0.5	Increase fracture toughness
Cu	< 0.55	Improves corrosion resistance Ferrite strengthener
Cr	< 1.25	In the presence of copper, increase atmospheric corrosion resistance
B	< 0.0005	Promotes bainites formation

To achieve the design requirements of strength and toughness properties, it is necessary to combine the practice of microalloying elements with special rolling routes and heat treatments.

3.2 Manufacturing of seamless pipes

There are two types of pipes in commercial use: welded, which are made of steel plates by welding, or seamless pipes, which are produced by hot working process without a welded seam. According to the API 5L standard [5], welding processes used for manufacturing of HSLA steels pipes can be categorized due to the use of filler metal, like submerged-arc welding and gas metal-arc welding, or without, as continuous welding, electric welding, and laser welding. Welded pipes usually have smaller cost, however seamless pipes have better mechanical load-bearing capacity and provide superior safety, because of its integrated structure, and better steel pipe geometry [9–11]. Therefore, seamless pipes are more likely to be used for offshore and sour applications.

Seamless pipes usually are manufactured according to the Mannesmann rolling process. This process uses a piercing mill, which is a skew rolling mill for piercing in cylindrical billets. While rotating the billet, with a high temperature, with a pair of skew rolls, the piercing mill presses the billet against a plug to pierce the billet, and then rolls the billet between rolls and the plug, forming it into a hollow tube of the prescribed outside diameter and wall thickness, as schematically shown in Figure 3.1 [4]. Afterwards, the pierced cylinder is cross rolled between the plug section of the mandrel and the rolls, further reducing the wall thickness [12].

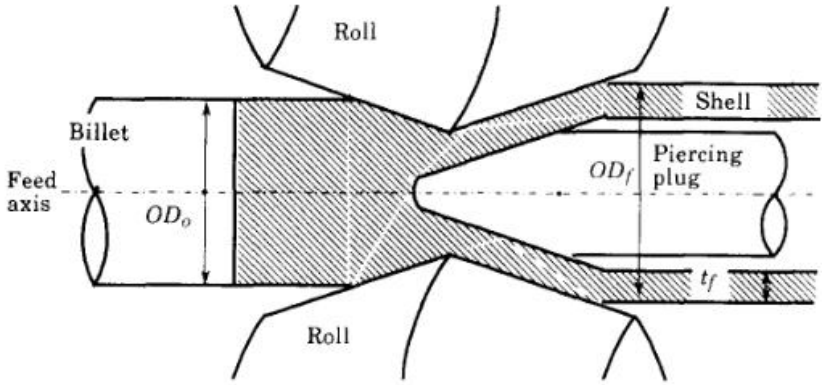

Figure 3.1 - Diagrammatic representation of the piercer [12].

According to Ling *et al*. [10], the production and deformation processes of seamless pipes are complex to control. Consequently, controlled rolling and controlled cooling are not enough to achieve the mechanical properties of higher grade seamless steel pipes such as X65 and X70 grades. Therefore quenching and tempering treatment are employed to produce seamless steels with this strength level.

According to Colpaert [13], quenching basically consists of a rapid cooling of a steel after heating it to an austenitizing temperature. As consequence, depending on the chemical composition, process and cooling rate, different constituents can be obtained. For example, for a X70 steel after off-line quenching, Ling *et al*. [10] obtained a microstructure mainly consisted of quasi-polygon ferrite with intragranular-ferrite (IGF) with pearlite, while, with an on-line quenching, it contained of intragranular-ferrite with lath bainite, as it can be seen in Figure 3.2.

According to Wu, *et al*. [11], one of the reasons to achieve diferent microstructures is that off-line quenching technology can obtain an equiaxed structure by re-austenitisation, while the original microstructure prior to the application of the on-line quenching technology is usually a deformed and pancaked austenite.

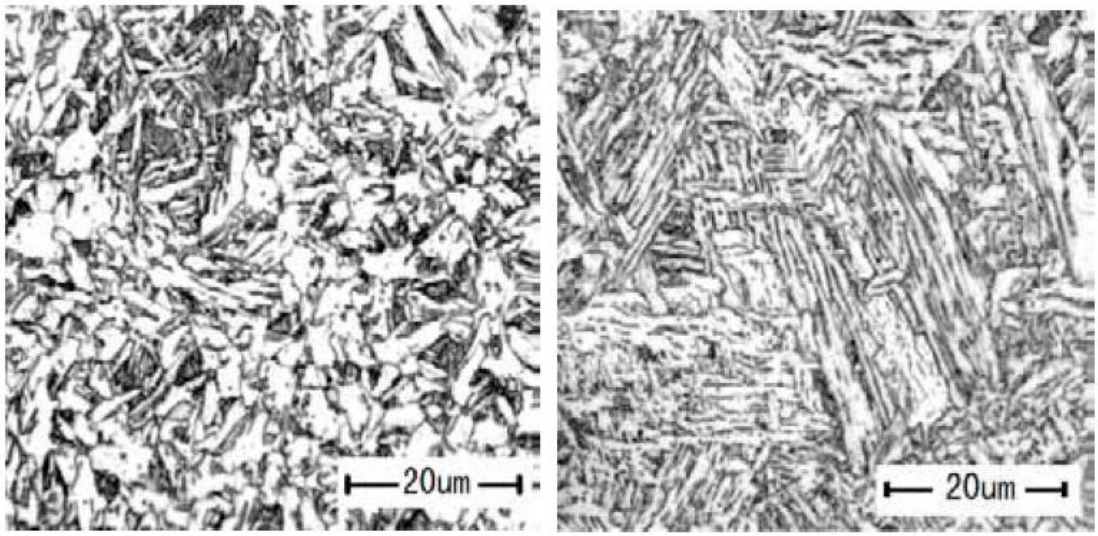

(a) (b)

Figure 3.2 – Microstructure of a X70 steel after (a) off-line and (b) on-line quenching [10].

A heat treatment known as tempering is usually carried out after quenching to promote stress relief and structural changes in the manufactured products to obtain adequate levels of strength and ductility. It involves the uniform heating of the quenched product up to a temperature just below the austenitizing temperature [13,14]. Jing *et al*. [15], studied the effect of four different tempering temperatures in the microstructe of pipeline steel X80 as shown in Figure 3.3. It is observed that at 550 °C and 600°C, the microstructure of X80 consists of bainitic ferrite (BF) + granular bainite (GB).

However, at the lower temperature, strip M/A constituent existed at the grain boundary and the interior sub-lath of some of GB commences to blend in such that their contours become undistinguishable. At the highest tempering temperature, the M/A constituent at grain boundaries is fully decomposed and bainite ferrite lath merges to form wide laths. Inner substructure of granular bainite disappears, M/A island turns into tiny and spotty particles because of gradual decomposition.

After being tempered at 650 °C and 700 °C, the microstructure of X80 is GB+QF (quasi-polygonal ferrite) and mainly QF, respectively. At the lowest tempering temperature, the original BF lath merges and recovers to form smaller GB crystal grain which refines the valid grain size. The M/A constituent in original granular bainite is decomposed to form fine M/A island and the ferrite matrix recrystallizes and changes into equiaxed QF.

As the second tempering temperature is higher, non-equilibrium microstructure that is formed by quenching sufficiently converts to QF which has lower free energy and grow up. Besides that, M/A constituent assembles, grows up and forms M/A constituent particles with large size at grain boundary of QF, which component with coarse M/A particles would be harmful to the toughness of X80 steel.

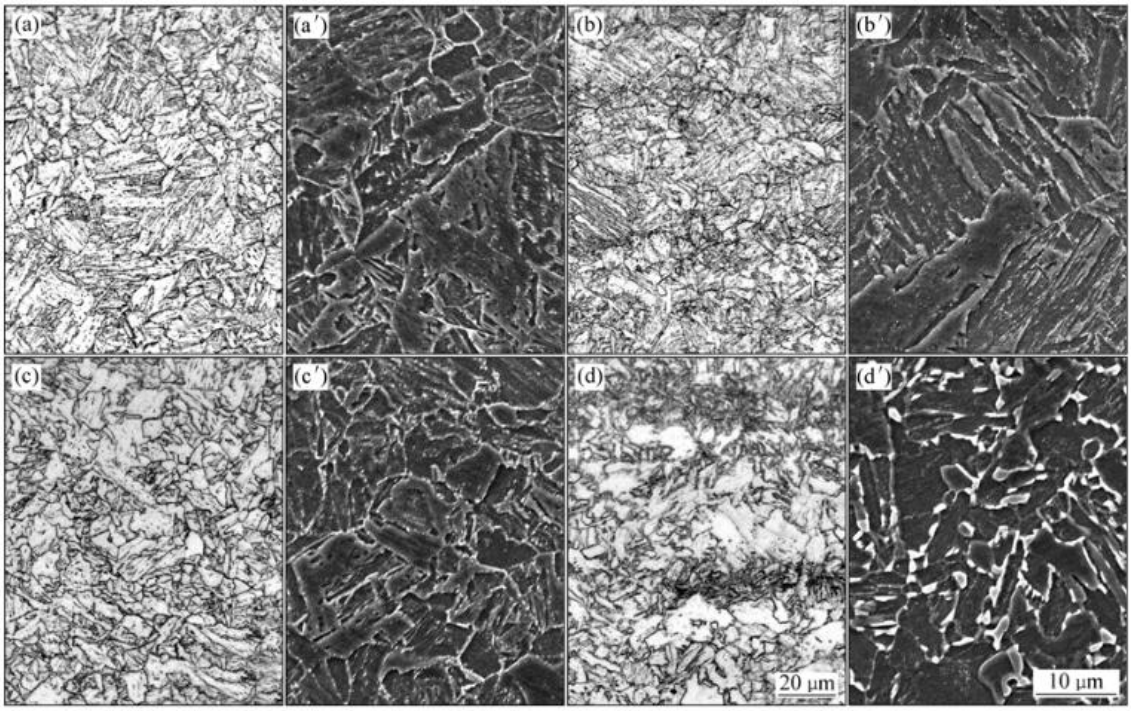

Figure 3.3 - Micrographs of X80 steel tempered at 550 °C (a) and(a'), 600 °C (b) and (b'), 650 °C (c) and (c'), 700 °C (d) and (d') [15].

3.3 Seamless pipes for offshore application

Oil and gas exploration and production in deep-water is associated with the use of highly sophisticated equipment and increasingly innovative technologies [16], as illustrated in Figure 3.4. Pipelines are a crucial part of the offshore industry, and it will likely remain so for the foreseeable future, as it constitutes the safest method to export and transport liquid and gaseous petroleum products or chemicals [17]

According to Bai [18], pipelines (and risers) are used for several purposes in the development of offshore hydrocarbon resources, that include:

- Export (transportation) pipelines;
- Flowlines to transfer product from a platform to export lines;
- Water or chemical injection flowlines;
- Flowlines to transfer products between platforms, subsea manifolds and satellite wells;
- Pipeline bundles.

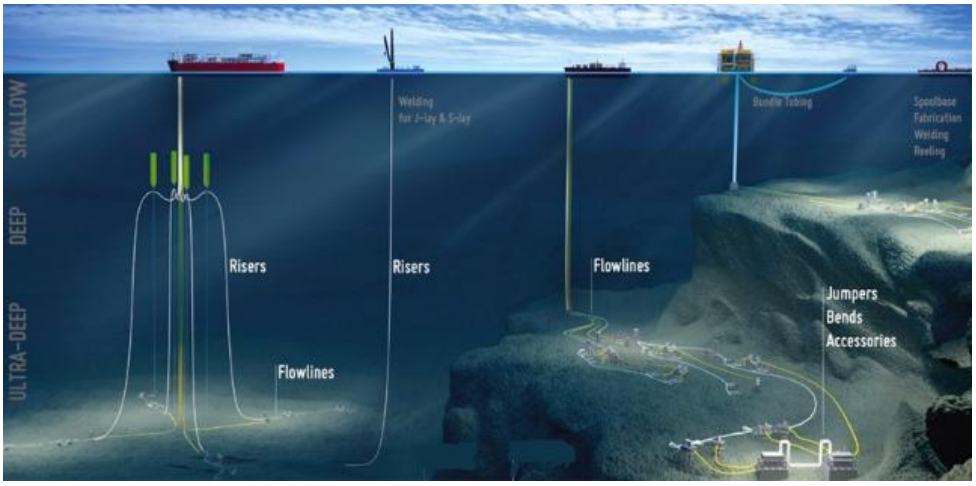

Figure 3.4 - Use of pipelines in the offshore industry [19]

Along the seabed, pipelines may be installed in potentially hazard environments and this operation involves impact, hooking and release of the pipeline by anchors or trawl gears, which is treated in the DNV GL guidelines [17]. This load cycle causes a complex stress and strain history that in turn may lead to fracture. This failure is unacceptable from an economical, ecological, and political point of view [20]. Therefore, studies and safety considerations are required to assess the hazards associated with possible accidents.

3.4 Fatigue in offshore pipelines

3.4.1 Pipe laying

According to Poberezhnyi *et al*. [21], there are two methods for offshore pipelaying that are more accepted worldwide: the S-method, which has been used for pipelaying at small depths, and the J-method, more suitable for deep waters. Figure 3.5 portraits a schematic representation for these methods of pipelaying.

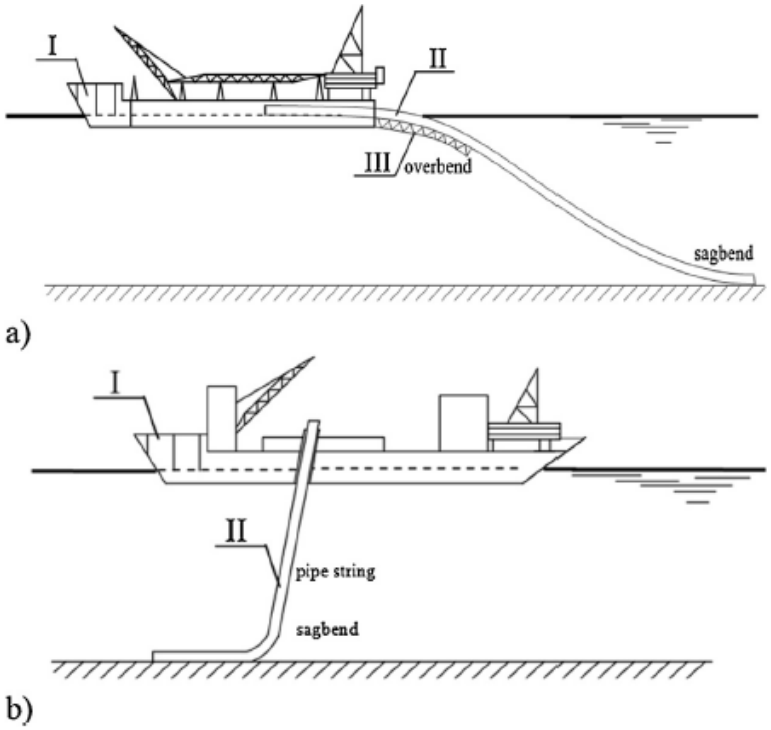

Figure 3.5 - Offshore pipelaying using (a) the S-method and (b) the J-method: I – pipelaying vessel; II – pipeline; III – stringer [21]

The S-lay conventional method of installation is named after the shape of the suspended pipe from the stinger to the seabed. Individual pipes are welded on the pipelay vessel and deployed horizontally over the stern down a stinger, a truss structure pinned to the fanner. It supports and guides the pipe as it enters the water which allows changing the angle of convergence and the curvature radius of the pipeline[21]. The pipe is held under tensile stresses as it leaves the vessel and, in the overbend section, it bends from horizontal to an almost vertical departure angle whilst leaving the stinger. This loading succession may permanently deform the pipe. Furthermore, environmental conditions may induce plastic straining in the pipeline due to action of cyclic stresses. The stresses need to be minimized and controlled to avoid failure due to fatigue cracking [22].

Similarly to the S-Lay, the J-method is named after the configuration of the pipeline during installation as it is deployed vertically into the water forming a “J” curve from the surface to the seabed. According to Senthil & Selvam [23], this technique uses a near vertical welding ramp in contrast to the horizontal system used in the S-lay. In this ramp, the pipes are also lowered at a near vertical angle to the seabed, which reduces the suspended span of pipeline and minimizes pipeline bending [21].

As consequence, this operation reduces the stresses applied in the tubes during laying which decreases the amount of plastic straining. For this reason, this technique has obtained prominence in the installation of rigid and fatigue sensitive pipelines in deep waters[23]. It should be however noted that the J-lay method is slower than the S-method and thus more costly.

Since 1944 during World War II, reeling is also used to install/construct offshore pipelines, especially for pipes having small to moderate external diameters (up to ~16") [24]. This laying procedure is considered one of the most efficient methods of pipe laying, as assembly, welding, inspection, and coating are conducted at onshore facility, diminishing both the time and the overall cost of installation [25].

The reel-lay procedure is briefly described as follows by Jia *et al*. [25], and Liu & Kyriakides [26]: First, in an onshore facility, the pipes are joined by girth welding into a pipeline with several kilometres in length. Afterwards, the pipeline is spooled onto a large diameter reel installed on a vessel. Finally, the vessel travels to the offshore facility where the pipeline is installed on the sea floor by spooling off from the reel, as shown in Figure 3.6. Nevertheless, reeling and unreeling induce large plastic strains in the pipes which may reach 1–3%. Thus, Engineering Critical Assessment (ECA) must be conducted accurately to avoid cracking of girth welds during installation using this method.

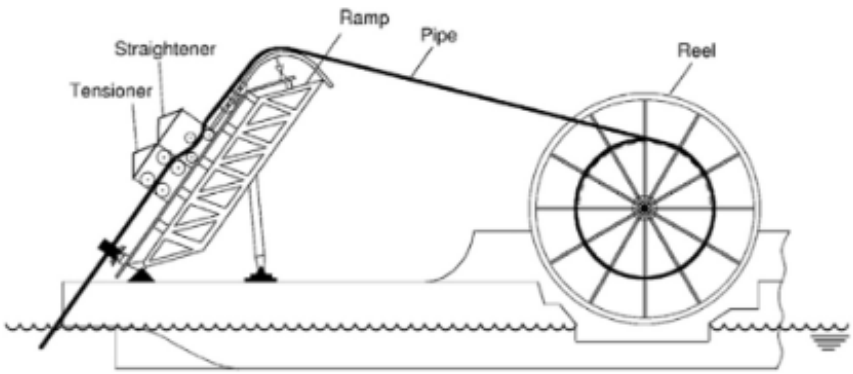

Figure 3.6 - Illustration of the reel-lay method [25]

3.4.2 Fatigue properties

Canadian Association of Petroleum Producers (CAPP) have reported several pipeline incidents in Canada from 1985 to 2008 and it have partitioned by causes, as it can be seen in Figure 3.7. Based on these documents, internal corrosion is the most dominant reason for leakage and failure for sour gas pipelines. However, under conditions of corrosion and combined cyclic stress, fatigue cracks often can be nucleated from corrosion pits that are geometric discontinuities which cause stress (or strain) concentration [27]. Therefore, the fatigue life of pipelines is one of the issues that needs to be considered to ensure their integrity and reliability.

According to Olamide *et al*. [29], the most important factors influencing the initiation and/or propagation of cracks in pipes and pipeline welds include their size, location and orientation, installation and operating conditions (i.e., high pressure and high temperature), material properties of the pipe and pipeline weld and geometry of the weld. Fatigue assessment where stable micro-crack growth occurs can be obtained based on the fracture mechanics approach to describe the fatigue behaviour of planar flaws such as cracks.

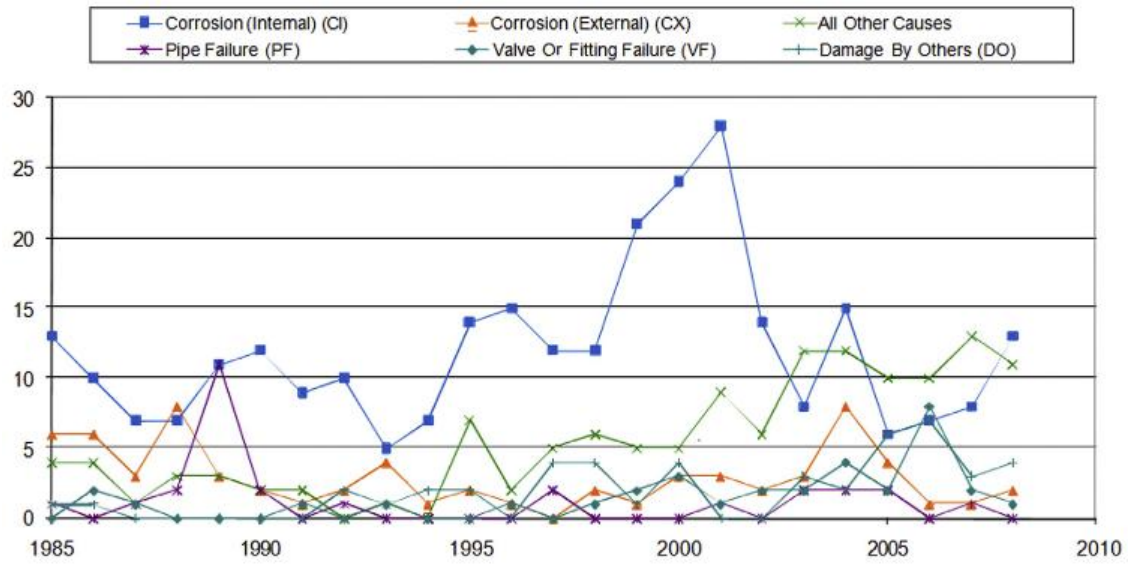

Figure 3.7 - Sour gas pipeline incidents by cause [28].

Fatoba & Akid [27], studied the behaviour of an API 5L X65 pipeline steel under low cyclic loading. It has been observed that increasing the total strain amplitude resulted in decrease of fatigue life and increase in stress and plastic strain amplitude, as shown in Table 3.3. Besides that, it was observed that, at all strain levels, final facture was at 45° to the direction of loading (Figure 3.8) and multiple cracks (white arrows in Figure 3.9) appeared on the periphery of the surface close to the fracture surface (red box in Figure 3.8) except for strain amplitudes of 0.3% and 0.5% where surfaces were smooth with no cracks.

Table 3.3 - Half-life strain-life low cycle fatigue results for API 5L X65 pipeline steel [27].

Strain amplitude (%)	0.3	0.5	0.65	0.8	1.0	1.2
Life (cycles)	13421	1466	1061	625	467	294
Stress amplitude (MPa)	416.4	453.2	475.8	491.1	531.3	536.3
Elastic strain amplitude	0.197	0.215	0.226	0.233	0.252	0.254
Plastic strain amplitude	0.103	0.287	0.428	0.568	0.745	0.938

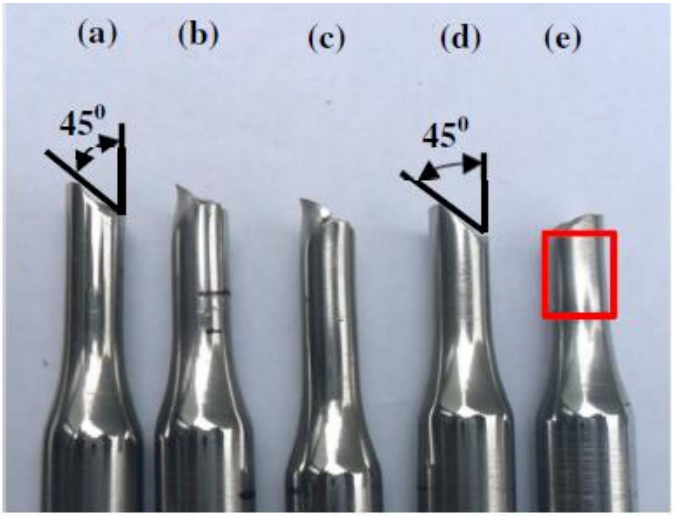

Figure 3.8 - Fracture surface morphologies of test specimens. Total strain amplitude = (a) 0.3%, (b) 0.5%, (c) 0.8%, (d) 1%, (e) 1.2% [27].

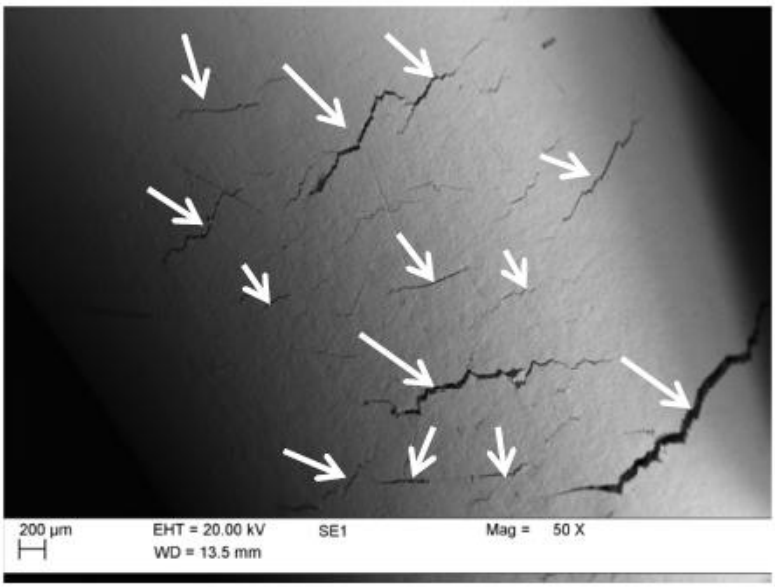

Figure 3.9 - View of surface periphery of specimen after testing showing multiple-site cracking. (Total strain amplitude of 1.2%) [27]

Fractographic results obtained by Fatoba & Akid [27], showed that fracture surfaces depicted evidence of crack initiation, crack propagation and overload zones. Scanning Electron Microscopy (SEM) analysis of damaged features also showed striations and cleavage-like facets in crack propagation zone while ruptured dimples and microvoid coalescence were detected in the overload zone, as demonstrated in Figure 3.10.

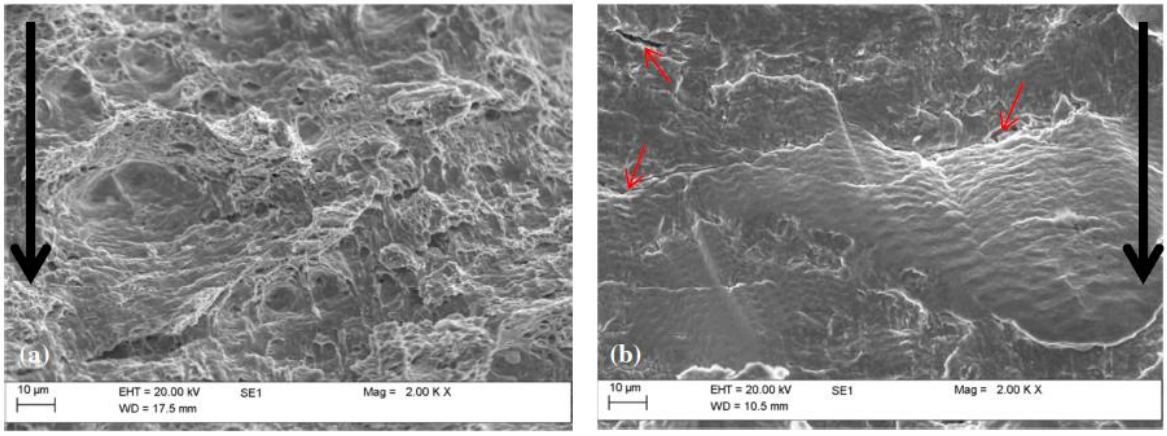

Figure 3.10 - High magnification SEM image of (a) overload zone (b) crack propagation zone on fracture surface of specimen cycled at 1.2% strain amplitude. The direction of crack propagation is highlighted with black arrows [27]

3.5 Fatigue analysis based on *S-N* data

Fatigue testing is the main procedure used for tackling the relationship between the fatigue resistance of a given material, component or structural detail and cyclic loading. The results of fatigue tests are plotted on graphs associating applied loading (force, stress, strain, etc) and the number of cycles to failure. Since the specimens and testing conditions are never identical, the resulting data are invariably scattered. Consequently, a detailed statistical analysis is required when using them to establish the required relationship [30]. According to the DNV-RP-C203 standard, a fatigue appraisal, based on S-N data obtained from fatigue tests, should be carried out for each individual member of the pipeline system to ensure that the structure will fulfil its intended functions [31].

Most of the *S-N* data are derived from fatigue testing of small specimens in laboratories until their ultimate failure. In these specimens, there is no possibility for redistribution of stresses during crack growth. This means that most of the fatigue life is associated with growth of a small crack that grows faster as the crack size increases until fracture [31]. When this failure criterion is transferred into real structures, redistribution of stress is more likely to occur, leading to a later failure compared with tests in smaller specimens.

DNV-RP-C203 standard [31] classifies each material according to construction details at which fatigue cracks may potentially develop. Hollow sections fabricated without welding (seamless pipes) using a high strength steel belong to class B1, such that their fatigue strength depends on the surface finish and the yield strength of the material. Materials with Submerged Arc Welding (SAW) and positional welds made by any process are class E and for single-side welds made on permanent backing are class F. According to [33], it is common to use class F in the pipeline design and analysis.

Considering the fatigue analysis based on nominal *S-N* curves, the loading is expressed as a stress range, *S*, and the fatigue resistance is expressed as the number of cycles, *N*, endured by the test specimen. In general, the same methods can be applied to fatigue endurance test results expressed using any measure of the loading (e.g. force, strain) and results obtained under loads having variable amplitudes [30].

According to Schneider & Maddox [30], there is a linear relationship between log *S* and log *N* as expressed in Eq. (1):

$$\log N = \log A - m \log S \qquad \text{Eq. (1)}$$

where *m* is the slope and log *A* is the intercept. Therefore, it can be re-written in a form that is commonly used to describe *S-N* curves in design rules:

$$S^m * N = A \qquad \text{Eq. (2)}$$

This assumption will only hold true for certain limits of stress amplitudes, as illustrated in Figure 3.11. The lower limit on *S* is determined by the fatigue endurance limit (or just 'fatigue limit'), such that fatigue failure will not occur for lower stress ranges. In practice, this is usually chosen based on the endurance that can be achieved without any evidence of fatigue cracking, typically for $2 \times 10^6 < N < 10^7$ cycles. The upper limit of *S* depends upon the static yield strength of the tested material and is commonly taken to be the maximum allowable static design stress [30].

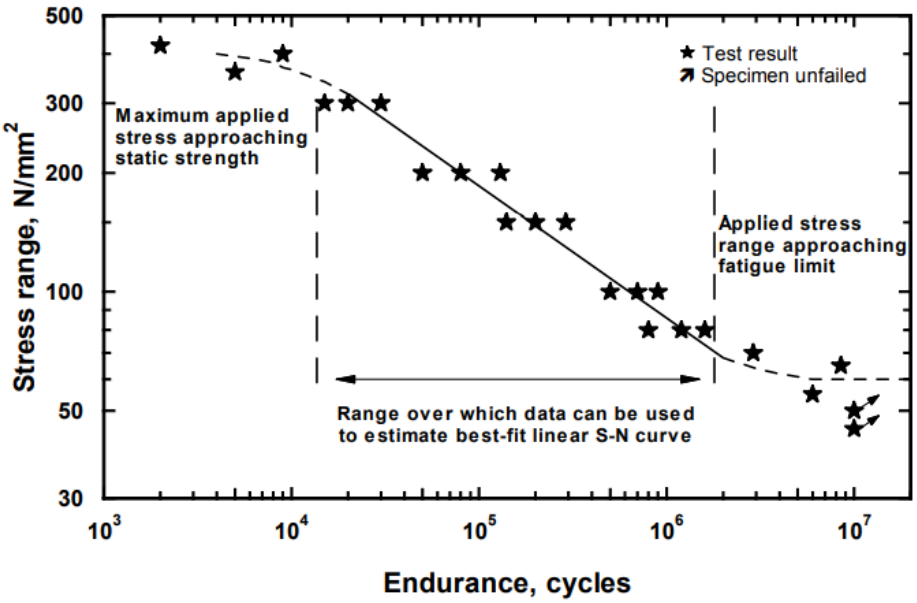

Figure 3.11 - Typical fatigue endurance test data illustrating deviations for a linear S-N curve [30].

According to Schneider & Maddox [30], *S-N* data comprise *n* data points ($logS_i$, $logN_i$), where S_i is the stress range and N_i is the endurance in cycles. This endurance is either the number of cycles to failure (or some pre-determined criterion, such as the attainment of a particular size of fatigue crack) or the number of cycles endured without failure. Figure 3.12 shows an example of such data, with some fitted *S-N* curves.

For design purposes, it is necessary to establish limits among which lies a given proportion of the data (typically 95%). These bounds are often termed 'confidence limits'. The two-sided 95% prediction limits are symmetrical, so there is a confidence of 97.5% of exceeding the lower limit −95% log N . This lower limit is thus equivalent to a lower one-sided 97.5% prediction limit, and it forms the basis of the most widely used fatigue design curves [30,31].

Fatoba & Akid [33], obtained, for a X65 steel pipe in air, the stress-life (*S-N*) endurance curve as presented in Figure 3.13 for specimens in high cycle fatigue. It is revealed that there is a limiting stress range (fatigue limit) of $\Delta\sigma$ = 450 MPa below which specimens did not fail.

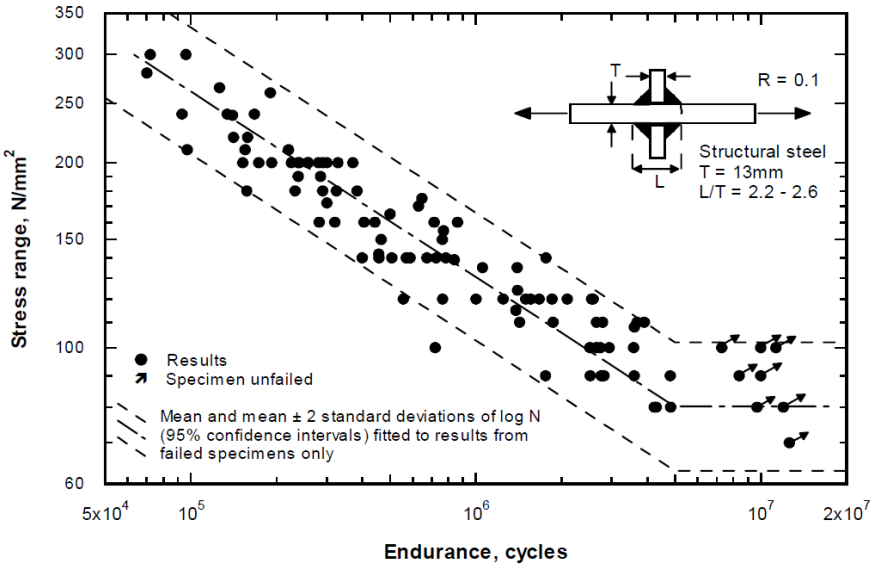

Figure 3.12 - Example of S-N data [30].

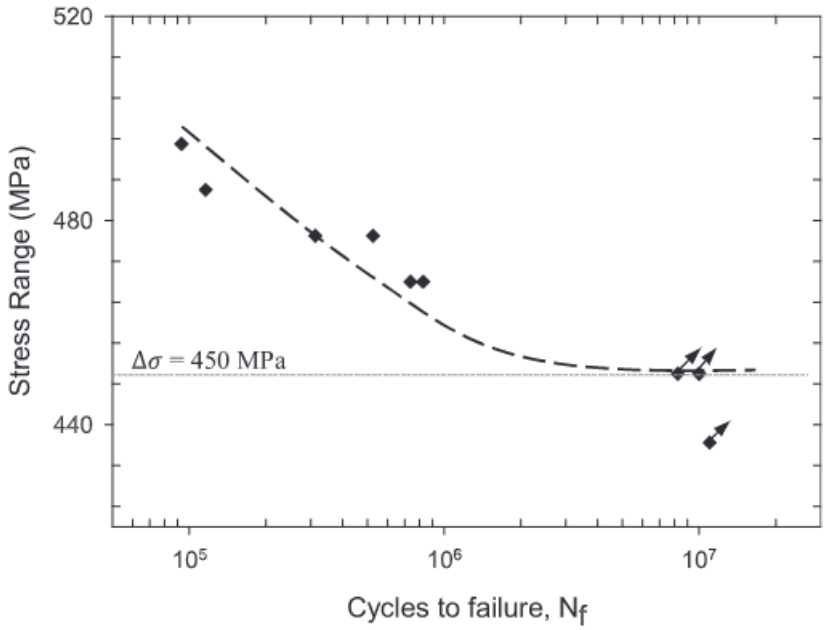

Figure 3.13 - Stress-life (*S-N*) curve for X65 steel in air [34]

4 METHODOLOGY

This chapter outlines the materials and methods used to evaluate the impact of grinding operations on the fatigue life of seamless pipes. It begins by providing information on the chemical composition and mechanical properties of the materials used in the study. It then presents the equipment and experimental procedures used. Finally, it provides a detailed description of the tests conducted to examine fractures in the pipes. Figure 4.1 shows a flowchart summarizing the steps of the activities conducted in this investigation.

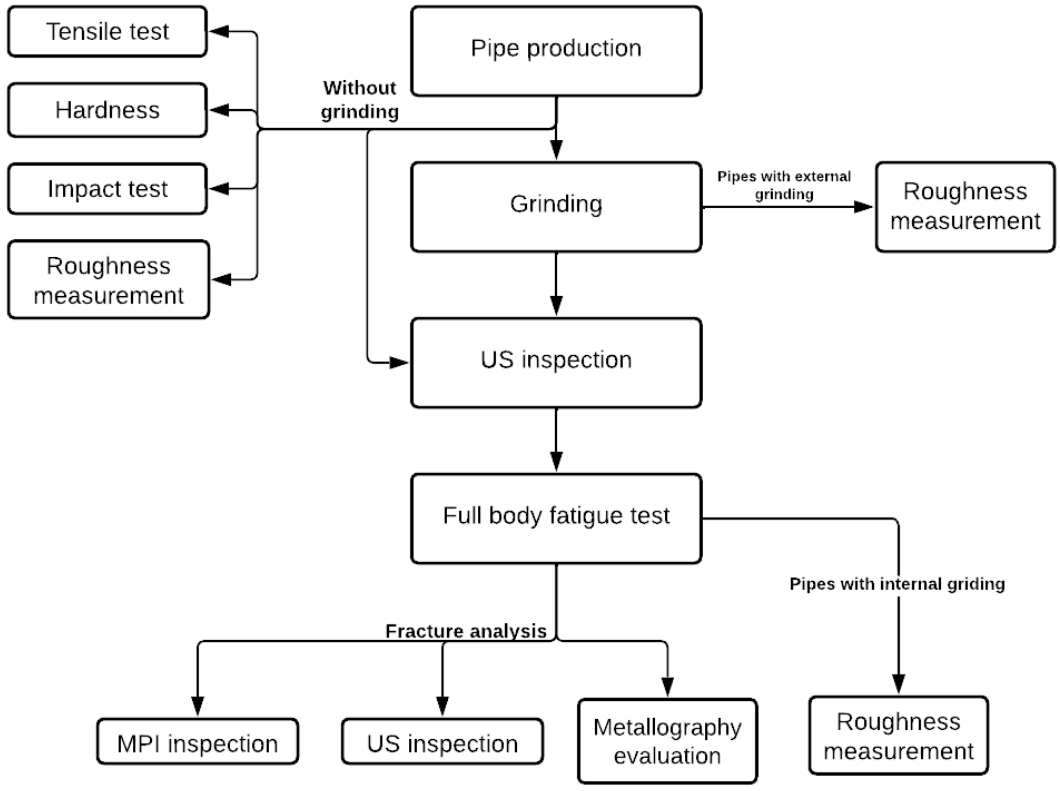

Figure 4.1 – Flowchart of the activies selected in this work.

4.1 Material

This study was carried out with a high-strength low-alloy steel for offshore and sour service application. Therefore, it was used seamless pipes in steel grade X65QO/X65QS PSL2 were designed in accordance with the standard API 5L, 2018 [5], whose chemical composition shall reach the requirements shown in Table 4.1.

The pipes selected for this investigation were fabricated through hot rolling followed by quenching in water and tempering. The seamless pipes display a nominal external diameter of 273.1 mm, a nominal wall thickness of 25.4 mm and a length of approximately 12.000 mm. The range of mechanical properties stablished for this grade of steel are presented in Table 4.2. The material shall also display a minimum average absorbed energy of 27 J and each test shall exhibit a minimum absorbed energy of 20 J (from a set of three test pieces).

Table 4.1 - Specified chemical composition for seamless pipe X65QOS according to standard API 5L (2018)

	Chemical composition (% in weight)								Carbon equivalent (CE) % max	
	C	Si	Mn	P	S	V	Nb	Ti	CE_{IIW}[3]	CE_{Pcm}[4]
X65QOS[1, 2, 3]	0.16	0.45	1.65	0.020	0.003	0.09	0.05	0.06	0.42	0.22

[1] $Al_{total} \leq 0.060\%$; $N \leq 0.012\%$; $Al/N \geq 2{:}1$; $Cu \leq 0.35\%$; $Ni \leq 0.30\%$; $Cr \leq 0.30\%$; $Mo \leq 0.15\%$; $B \leq 0.0005\%$

[2] $Nb + V + Ti \leq 0.15\%$

[3] $CE(IIW) = \%C + \frac{\%Mn}{6} + \frac{\%Ni+\%Cu}{15} + \frac{\%Cr+\%Mo+\%V}{5}$

[4] $CE\ (Pcm) = \%C + \frac{\%Si}{30} + \frac{\%Mn+\%Cu+\%Cr}{20} + \frac{\%Ni}{60} + \frac{\%Mo}{15} + \frac{\%V}{10} + 5 * \%B$

Table 4.2 - Mechanical properties specified for grade X65QOS as per API 5L (2018)

Yield Strength (YS)	Tensile Strength (TS)	Elongation	Hardness
450 – 570 MPa	535 – 760 MPa	A_f[1]	≤ 250 HV10

[1] $A_f = 1940 * \frac{A_{xc}^{0.2}}{U^{0.9}}$ where *Axc* is the applicable tensile test piece cross-sectional area (mm^2) and *U* the specified minimum tensile strength (MPa).

4.2 Grinding

A total of six (6) seamless pipes were selected for the conduction of grinding at their inner surfaces. This procedure was performed along the entire perimeter of each pipe at three different positions along its length, taken at 3.5, 4.0 and 4.5 m of the tip of the tube, as illustrated in Figure 4.2 with the ground regions, in gray. This procedure was carried out using a Norton grinding wheel composed by a resinoid alloy with aluminum oxide abrasive having a granulometry 16 (Figure 4.3). The grinding wheel displays an outer diameter of 57.20 mm and an inner diameter of 31.80 mm. The grinding operation, as demonstrated in Figure 4.4, has initiated with the grinding wheel positioned 100 mm away from the reference point and the wheel was displaced longitudinally for a total of 200 mm.

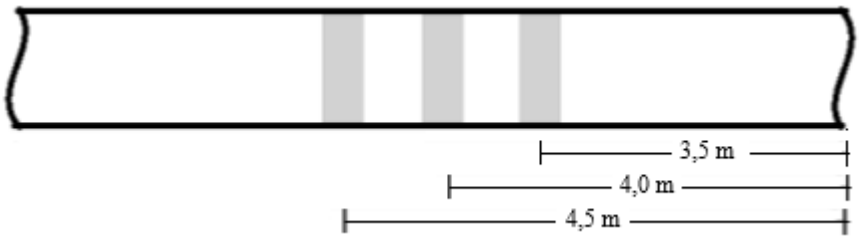

Figure 4.2 – Representation of the ground regions in the seamless pipes.

Figure 4.3 - Grinding wheel used in the automatic repair operation on the inside pipe surface.

Figure 4.4 - Grinding operation at the inner surface of the pipe.

The grinding operation was set with the following processing parameters:

- Rotation speed of grinding wheel: 4500 rpm;
- Rotation rate of the pipe: 2250 rpm;
- Lance speed of moving: 90 mm/s
- Three (3) passes (forth/back/forth);
- Operation performed without lubrication (dry grinding).

Six (6) pipes fabricated with the same heat treatment parameters were selected to study the fatigue endurance without the effect of any repair grinding. Furthermore, an operation of manual grinding at the same positions previously described but at the outer surfaces was selected for two (2) additional seamless pipes to examine the effect of external grinding. The operator was not provided with an orientation regarding the grinding direction (longitudinal or transverse) in the procedure. Consequently, the operator made the decision during the operation.

4.3 Ultrasonic inspection

An ultrasonic inspection was performed in the seamless pipes to check if there were any remaining surface defects. This inspection was performed according to the standard API 5L (2018) [5]. Therefore, for sour and offshore application, the maximum depth of longitudinal surface imperfections shall be 5% of the specified wall thickness and, for laminar imperfections, the maximum individual imperfection area is 500 mm². Larger imperfections are classified as defects which shall be cut off or repaired by grinding. Inspection of the pipes was also used to examine whether the wall thickness was between 22,40 to 29,10 mm along the pipe length, as demanded in the API 5L (2018) [5] standard.

In order to allow additional tests, after the ultrasonic inspection, it was removed a sample of 380 mm from one extremity of both pipes with external grinding. Then, it was adjusted pipe length to 8.000 (-0/+100) mm from the extremity measured the grinding operation and, after that, it was removed another sample of 380 mm from the middle of the pipe. Pipes with internal grinding were also adjusted to the same length considering the extremity measured the grinding operation. Pipes without grinding was also adjusted to length of 8.000 (-0/+100) mm.

4.4 Roughness analysis after external surface grinding

Roughness measurements were conducted at the outer surface on the samples removed from the middle of the pipe and on the area with the external grinding to assess the impact of the grinding operation in their tribological properties. The roughness was recorded using an automatic rugosimeter SJ-310 Mitutoyo (see Figure 4.5) certified according to ISO 1997. The measurements of the average roughness (Ra) were recorded longitudinally three time at each position. Four positions were considered along the perimeter of each pipe, separated by an angular distance of 90°.

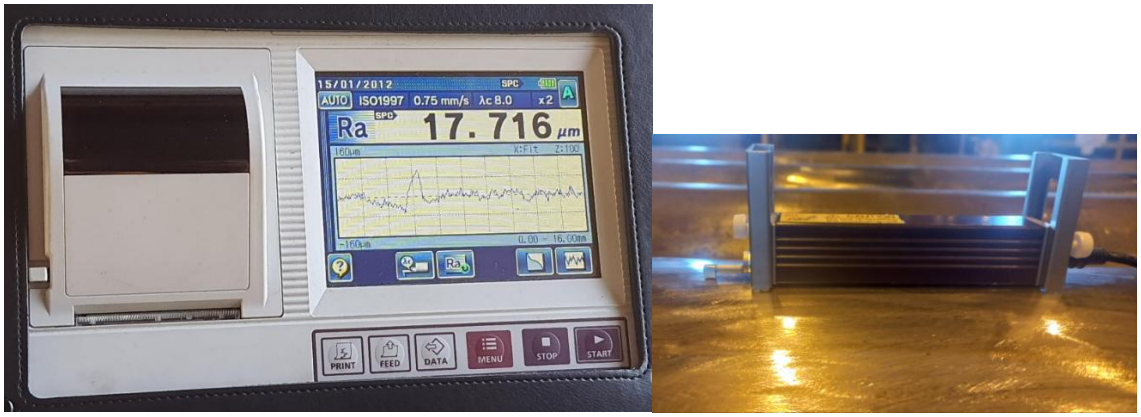

Figure 4.5 - Rugosimeter used to measure the surface roughness of the seamless pipes

4.5 Full-scale resonant fatigue testing

For each configuration, a set of 3 stress amplitudes were used which is consistent with API 17G [36]. However, specimens' length was shortened to 6.5 m due to load frame constraints. In order to confirm the integrity of the pressurization system, all specimens were first proof tested using a hydrostatic pressure of ~1.2 times the pressure selected for the fatigue tests. At this stage, the pipes were filled via tapping at one end plug. The liquid was then vented via a tapping in the pipe wall close to the other extremity of the pipe such that the volume of any trapped air was reduced to a minimum.

As the specimens can potentially fail anywhere within the central third of the specimen, it was important to measure the distribution of strain throughout this region. This procedure involved two stages:

- Firstly, the strain gauges 1-8 were distributed around the circumferential center of the specimen.
- Secondly, the variation of strain along the length of the specimen were recorded using the strain gauges 9-16 positioned over 2,200 mm in 8 different planes, as represented in Figure 4.8. For consistence purposes, the same monitoring procedure was undertaken on pipes without any repair.

Therefore, all strain gauges were positioned as illustrated in Figure 4.6.

Figure 4.6 – Representation of the strain gauges 9-16 position vs. areas of interest on ID repaired specimens

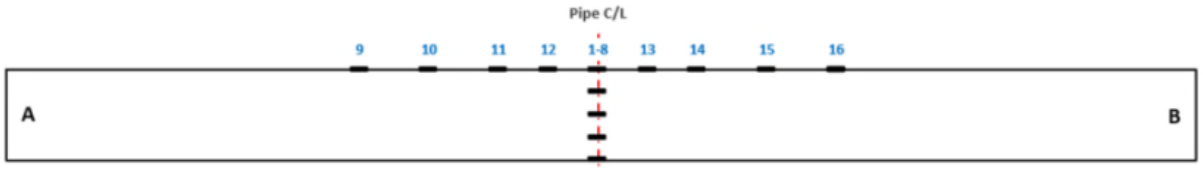

9	10	11	12	1-8	13	14	15	16
- 1 100	- 750	- 500	- 250	-	+ 250	+ 500	+ 750	+ 1 100

Figure 4.7 – Representation of the position of all strain gauges

The specimens were tested in air, at room temperature (*RT*), in Vallourec designed resonance fatigue machine. These systems permitted the imposition of a rotating alternating bending moment, at a frequency of 20-25 Hz, which was selected based on the latest studies conducted at Vallourec.. The testing speed was finely controlled to achieve a constant stress amplitude throughout the test and set so that the average of the readings recorded in the strain gauges 1-8 corresponded to the required stresses. The test conditions undertaken in the current investigation are outlined in Table 4.3. The tests were terminated upon through-wall cracking detected by a drop in internal pressure, or as runouts if failure did not occur up to 2×10^7 cycles which could be close to the fatigue endurance limit. Besides that, this corresponds to conditions of high cycle fatigue.

With the mean S-N curve for the class selected, it was calculated the S-N curve validity assuming 5% significance level with the following formula according to BS 7608 [35]:

$$\log \overline{N_{test}} = \log N_d + \frac{1.645.SD_d}{\sqrt{n}}$$

where:

$\log \overline{N_{test}}$ is the mean logarithm of the fatigue life from the tests at a particular stress;

$\log N_d$ is the logarithm of the corresponding fatigue life from the mean S-N curve for the design class;

n is the number of fatigue test results.

SD_d is the standard deviation for the database that produced the design curve

Validity would be evaluated for each separate fatigue level and then consolidated at average. The obtained factor should be greater or equal to 1.645 to validate significance level below 5% i.e., it is more than 95% likely that the considered data points belong to a class that is equivalent or better than the one it is checked against.

Table 4.3 - Fatigue test conditions of each specimen

	Reference specimen	Hydrotest		Fatigue test	
		Time (s)	Pressure (MPa)	Stress range (MPa)	Pressure (MPa)
No grinding	R159-01	60	73,4	240	61,2
	R159-02	60	73,4	240	61,2
	R159-03	60	73,4	240	61,2
	R159-04	60	61,2	200	51,0
	R159-05	60	61,2	200	51,0
	R159-06	60	61,2	200	51,0
ID grinding	R159-07	60	73,4	240	61,2
	R159-08	60	73,4	240	61,2
	R159-09	60	61,2	200	51,0
	R159-10	60	61,2	200	51,0
	R159-11	60	55,1	180	45,9
	R159-12	60	55,1	180	45,9
OD grinding	R159-13	60	61,2	200	51,0
	R159-14	60	61,2	200	51,0

4.6 Post-fracture analysis

Following the full-scale fatigue test, each specimen was submitted to an ultrasonic inspection to identify only the location of failure within the repaired area.

Additionally, the roughness of the internal surface of specimens R159-07 to R159-12 (with internal grinding) was measured. The internal surface was first cleaned with a brush to remove as much as possible the rust that could affect surface quality analysis. Figure 4.8 displays the internal surface of specimen R159-11 after cleaning. Roughness was measured using a metrology station (APP-TDS-032: Station Altisurf 500R) on the internal surface, both with and without grinding.

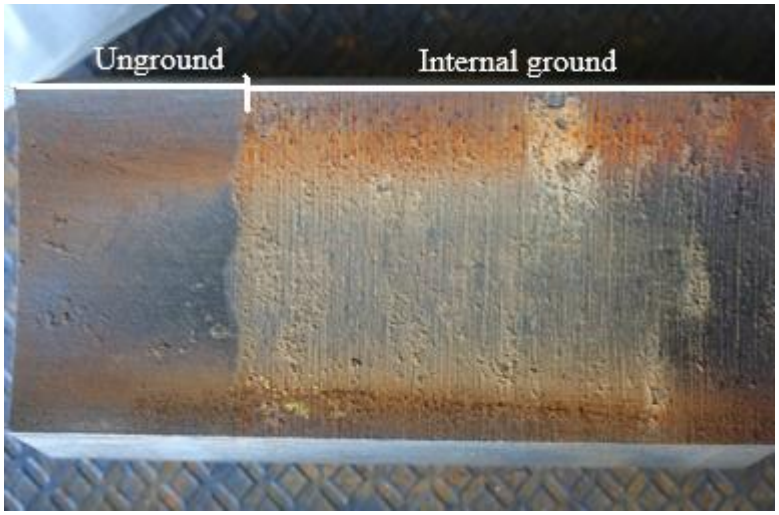

Figure 4.8 – Internal surface of the specimen R159-11 after surface cleaning

To assess whether repair operation promotes different cracking dynamics, first it was performed a magnetic particle inspection (MPI) in each specimen surface (external and internal) to identify indications of fatigue cracks. Then each specimen was cut closer to the longest MPI indication, to evaluate the fracture surface with macrography and SEM (Scanning Electron Microscopy).

5 RESULTS

5.1 Mechanical properties

After quench and tempering, tensile tests were carried out in strip specimens of 19,1 mm machined out at positions located along the length and circumference of the same pipe. Three positions were selected along the pipe length (the tube ends and its middle section). Also, two tensile tests were conducted for each longitudinal position, for specimens located at opposing quadrants (0° and 180°). The results obtained in the tensile tests are presented in Table 5.1.

Table 5.1 – The variations of the yield strength, tensile strength and elongation along at different positions along length and circumference of the hollow pipe.

	Yield Strength (MPa)	Tensile Strength (MPa)	Elongation (%)
		Position 0°	
Pipe Beginning	507	592	46
Pipe Middle	481	571	49
Pipe Bottom End	494	585	49
		Position 180°	
Pipe Beginning	500	590	49
Pipe Middle	504	592	49
Pipe Bottom End	489	576	48
API 5L requirement	450 - 570	535 - 760	> 23

A comparison of the tensile results shown in Table 5.1 reveals that there were no significant variations in the yield strength (YS), tensile strength (UTS), and elongation to failure along the circumference of the pipe, for the same longitudinal positions. At the circumferential position corresponding to $\theta = 0°$, maximum variations of 26 and 21 MPa in the YS and UTS, respectively, were recorded along the pipe length. For $\theta = 180°$, the differences in the YS and UTS vary within the range of 15 and 16 MPa, respectively. The aforementioned results thus suggest there is a reasonable homogeneity in the mechanical properties throughout the pipe.

Transverse impact tests were carried out with triplicate full size specimens (10x10) taken from three (3) different pipes for an average temperature of -40°C. The values of the absorbed energy and the fraction of areas showing shear features are presented in Table 5.2. It is readily seen that all results fulfill the requirements of API 5L 46th, 2018 [5] (minimum average energy of 27J and minimum individual energy of 20J). It is also apparent that the tested alloy exhibited high toughness at -40°C, as the average absorbed energy is consistently > 397 J and all tests depicted ductile failures (shear area = 100%).

Table 5.2 – The values of the absorbed energy and the fraction of areas showing shear features for transverse impact tests carried out at -40°C.

Specimen	Absorbed Energy (J)			Shear area (%)		
	Pipe 1	Pipe 2	Pipe 3	Pipe 1	Pipe 2	Pipe 3
1	403	404	423	100	100	100
2	418	384	416	100	100	100
3	413	404	416	100	100	100
Average	411	397	418	100	100	100

The hardness values were recorded using a Vickers indenter thickness of the tube at θ = 0 and 180°. The measurements were undertaken at a distance of ~1.5 mm from the inner diameter, at the mid-thickness and at a distance of ~1.5 mm from the outer diameter. Figures 5.1 and 5.2 display the average values of the Vickers hardness in each position, before griding, together with bars indicating the minimum and maximum values recorded. According to API 5L, 2018, [5] the maximum hardness shall be 250 HV10. In this study, the hardness values did not exceed 222 HV10 at θ = 0° for the inner diameter position and 237 HV10 at θ = 0° for the outer diameter position. Therefore, all results of hardness are in accordance with API 5L, 2018.

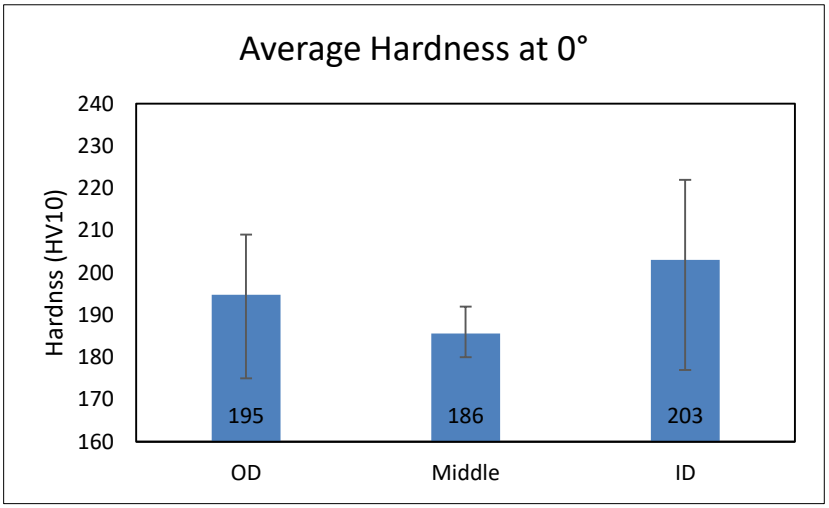

Figure 5.1 - Results of average hardness (HV10) in position 0° before grinding

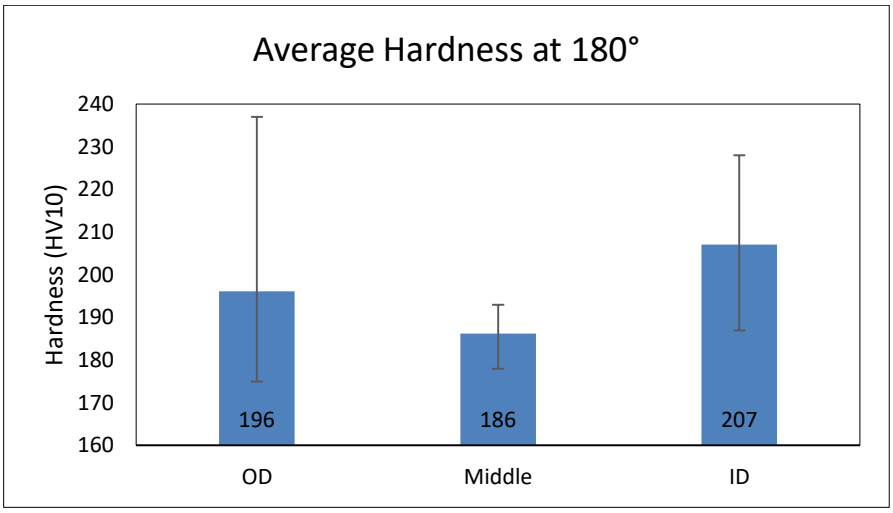

Figure 5.2 - Results of average hardness (HV10) in position 180° before grinding

Comparing the results of average hardness in the same position, it can be seen a small variation through pipe thickness, as it was obtained a variation of average hardness of 17HV10 in position 0° and 21HV10 in position 180°. Furthermore, comparing the results of average hardness in position 0° with in position 180°, it possible to notice that results are also similar, as for example, in the middle of the wall thickness, it was obtained the same average hardness.

Therefore, one can see that the pipes used in this project have a good homogeneity throughout the pipes, as presented with the results of tensile test, and also considering different pipes, as follows with the results of impact and hardness tests.

5.2 Wall thickness profiles

Ultrasonic inspection was performed to evaluate the integrity and overall quality of the pipe surfaces in order to identify remaining surface defects according to API 5L (2018) [5] requirements. It follows from the inspection results that any eventual longitudinal surface imperfection detected in the pipes displayed depths < 5% of the specified wall thickness. Also, any eventual laminar imperfection exhibited an area smaller than 500 mm². Therefore, all pipes were approved considering the quality surface condition required by API 5L (2018) [5].

The wall thicknesses were also measured along the pipe's length and each perimeter through ultrasonic inspection, as it can be seen in Figures 5.3 to 5.7. In those graphics, the horizontal and vertical axis represents the length (m) and the wall thickness (mm) of the pipe, respectively. The green lines correspond to the minimum and maximum wall thickness measured in each pipe section and the yellow line corresponds to the average wall thickness. The lower and upper dashed lines correspond to the wall thickness limits of 24.23 mm and 28.27 mm, respectively. It should be noted that all pipes displayed wall thicknesses within these limits, except the specimen 159-04 that showed a maximum thickness of ~29.00. Therefore, the pipes produced for the current study had thicknesses more restricted than the API 5L (2018) [5] requirements (from 22.40 to 29.10 mm).

Ground areas are clearly visible in Figures 5.5 to 5.7. It is evident from Figures 5.5 and 5.6 that pipes with internal grinding exhibit more noticeable ground areas due to a greater reduction in wall thickness near the ground area. It is worth noting that the grinding operation did not result in a smooth transition between the dressed area and the pipe contour. The reduction in wall thickness at the base of the pipes was less pronounced for pipes with external grinding, as indicated by the yellow line representing the mean wall thickness. Consequently, the dressed area blended more smoothly with the pipe contour.

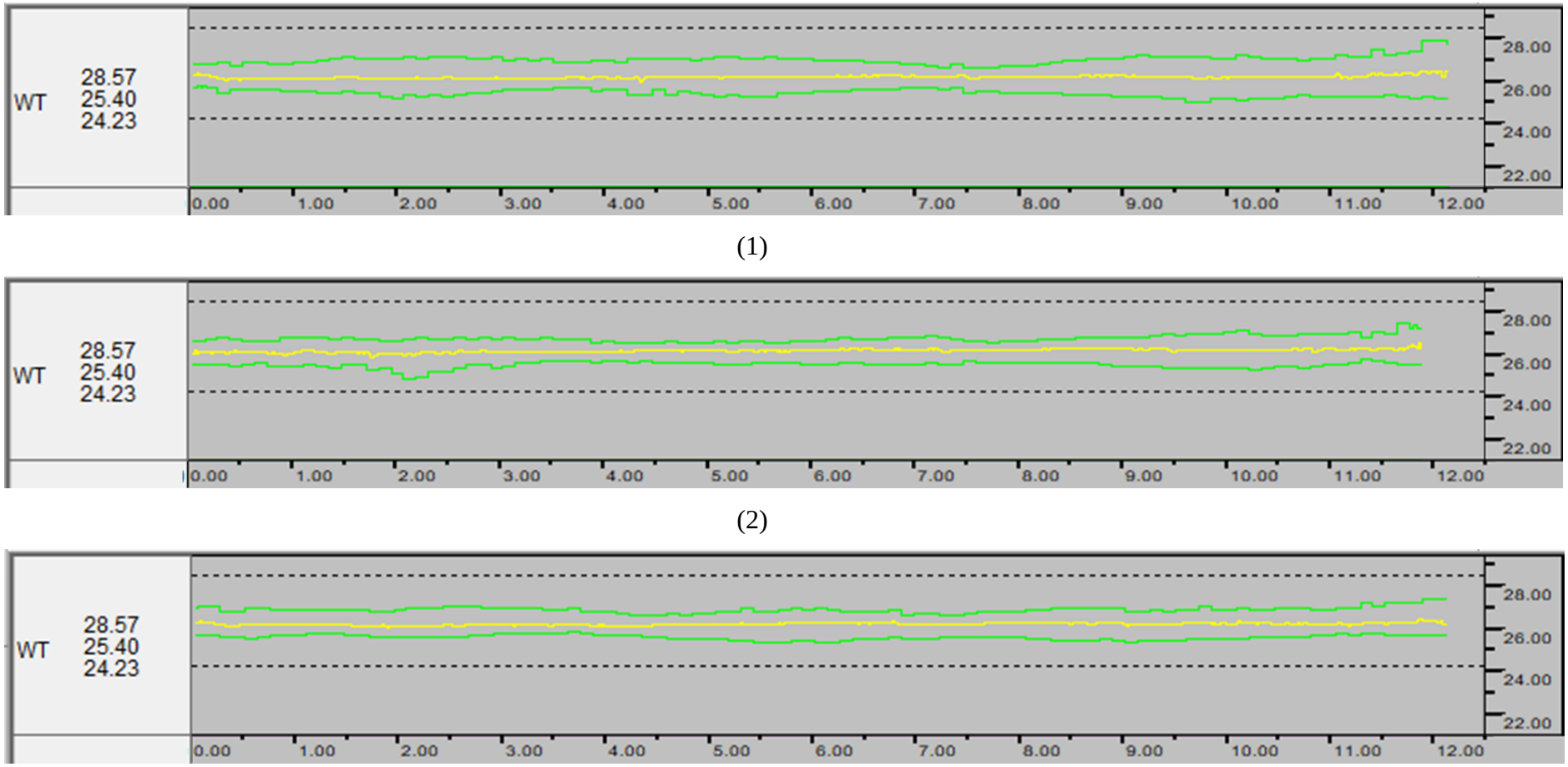

(1)

(2)

(3)

Figure 5.3 – Wall thickness measured by ultrasonic inspection along each pipe length without grinding: (1) 159-01; (2) 159-02; (3) 159-03

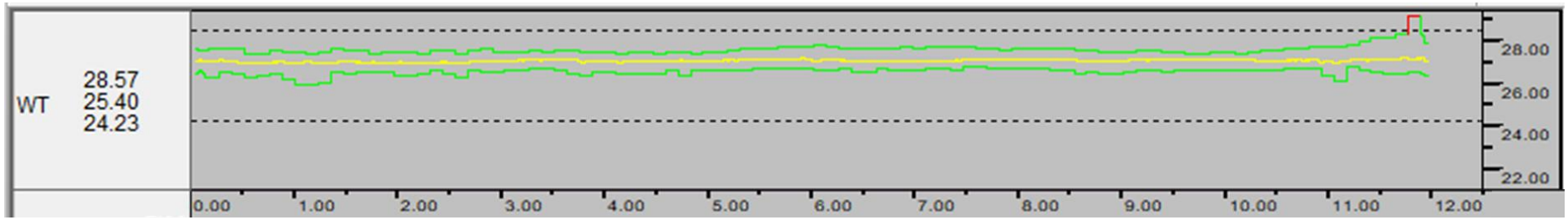

(1)

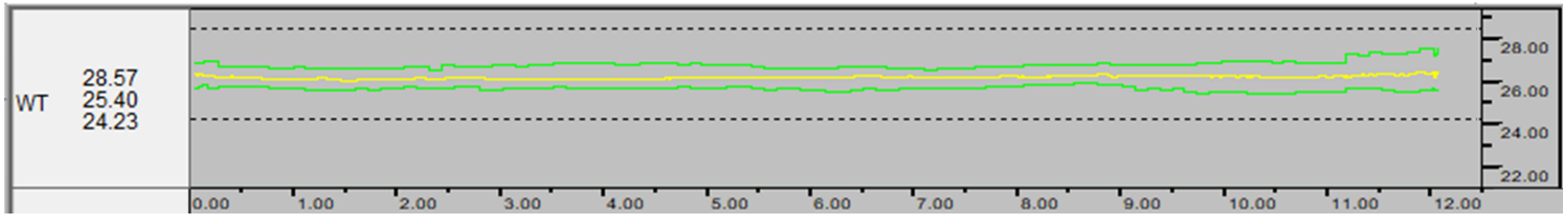

(2)

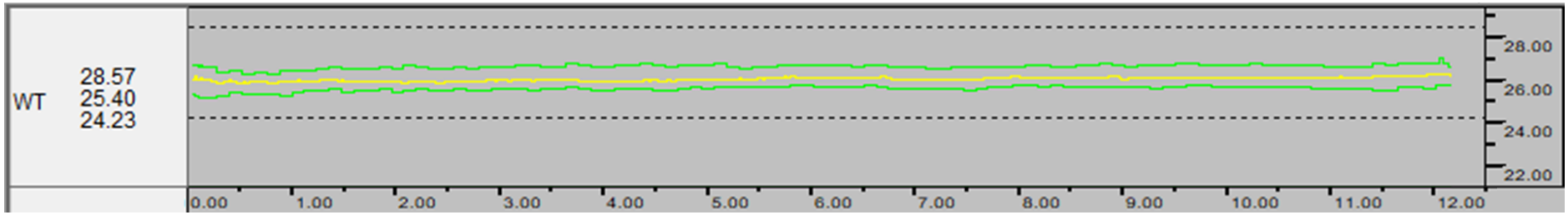

(3)

Figure 5.4 – Wall thickness measured by ultrasonic inspection along each pipe length without grinding: (1) 159-04; (2) 159-05; (3) 159-06

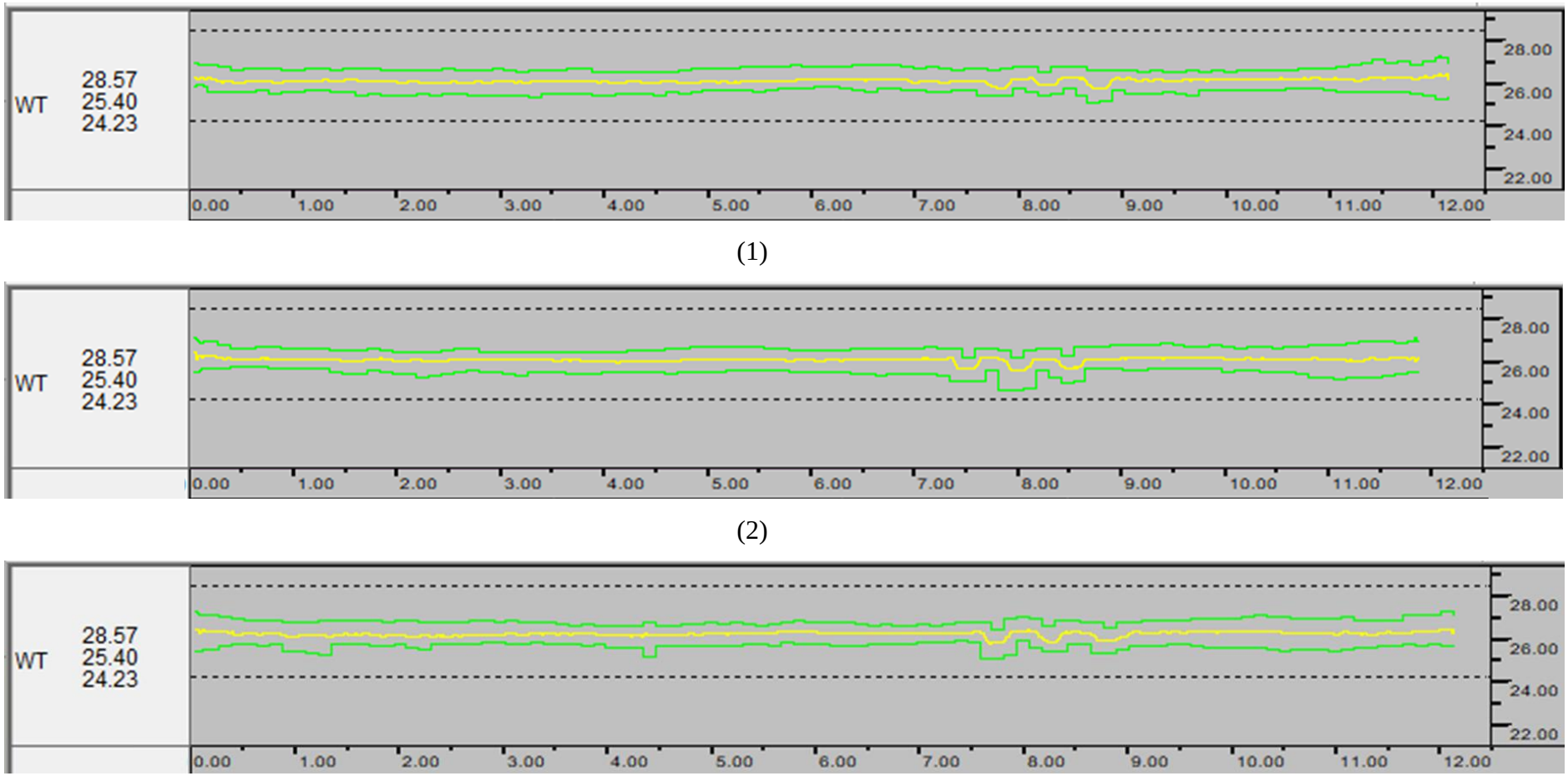

Figure 5.5 – Wall thickness measured by ultrasonic inspection along each pipe length with ID grinding: (1) 159-07; (2) 159-08; (3) 159-09

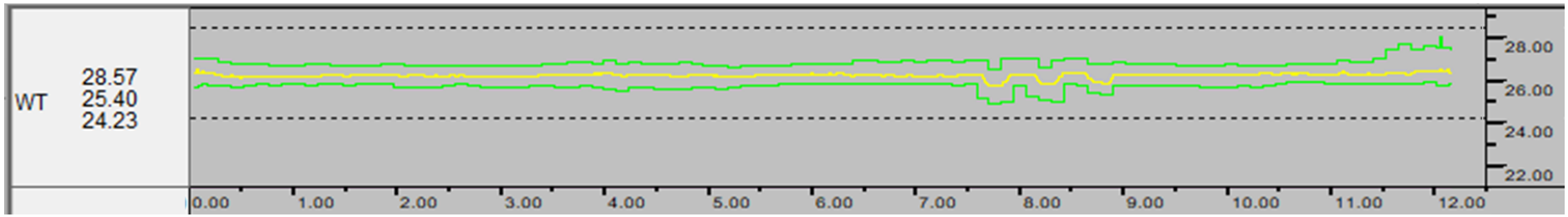

(1)

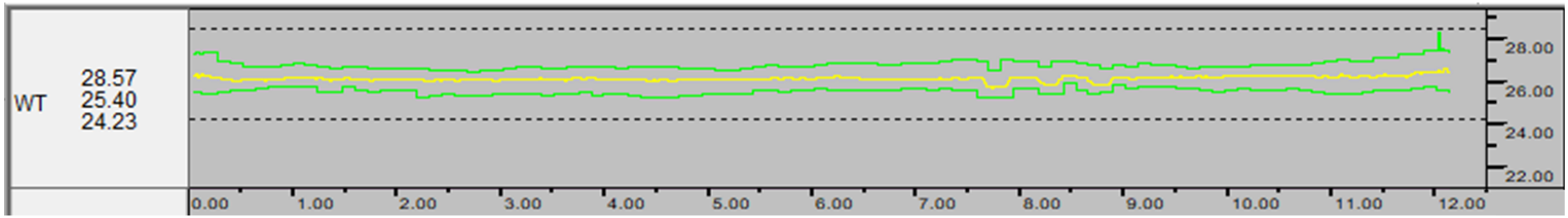

(2)

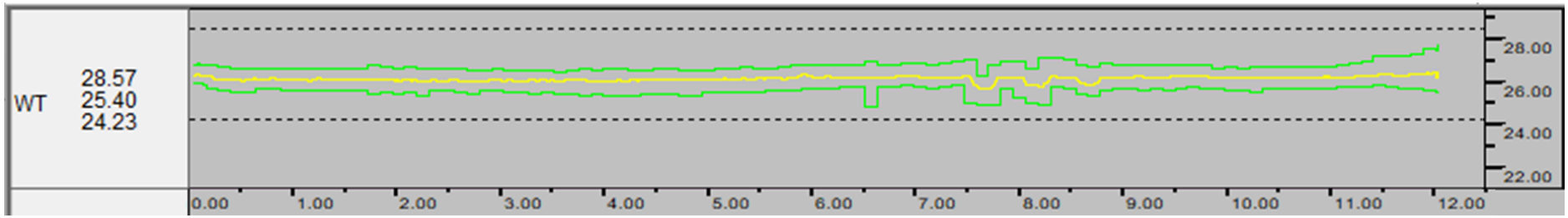

(3)

Figure 5.6 – Wall thickness measured by ultrasonic inspection along each pipe length with ID grinding: (1) 159-10; (2) 159-11; (3) 159-12

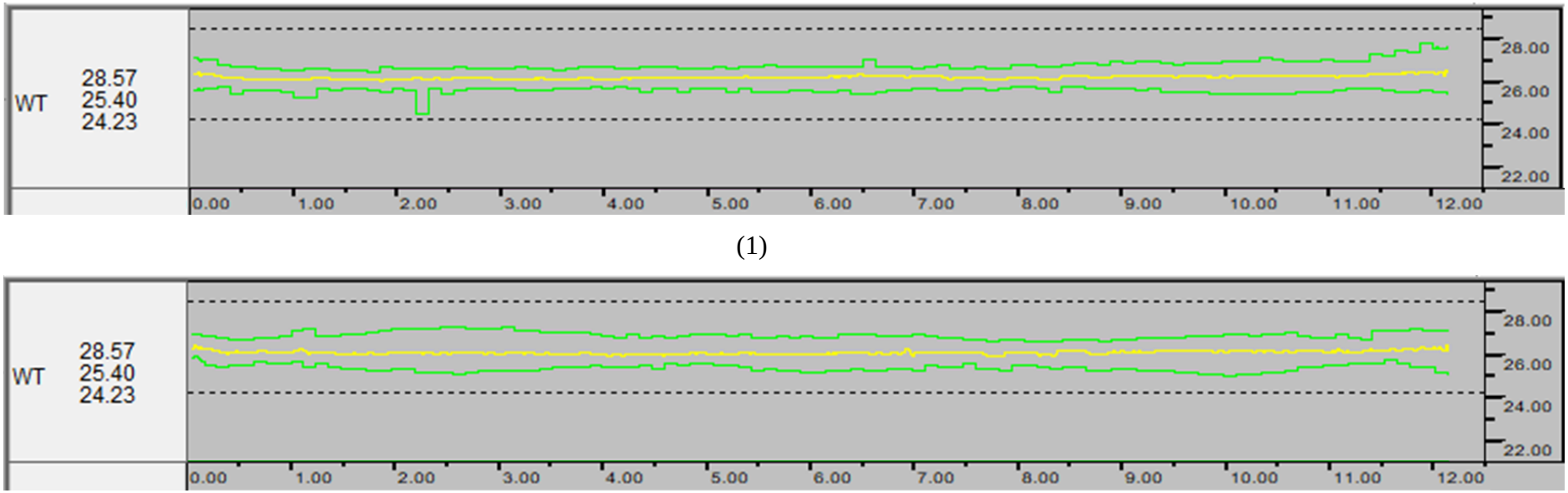

Figure 5.7 – Wall thickness measured by ultrasonic inspection along each pipe length with OD grinding: (1) 159-13; (2) 159-14

5.3 Average roughness after external surface grinding

The average roughness (Ra) was measured at four positions, 90° apart, on specimens 159-13 and 159-14, both with and without external grinding. Figure 5.8 displays the average roughness at each position, along with bars indicating the minimum and maximum standard deviation in each condition. In the unrepaired region, the average roughness ranged from ~5.05 to 6.76 µm. The region where manual grinding was performed on the external surface displayed a decrease in average roughness to values between ~0.94 and 1.10 µm. This demonstrates the effectiveness of manual grinding in reducing the roughness of the steel pipes.

It follows from the Ra values shown in Figure 5.8, there was no representative variation in roughness along the pipe perimeter regardless the surface finishing condition. It is worth noting that the variability appears to decrease even further in the pipes which underwent external grinding, as there was a significant reduction in the standard deviations. These findings demonstrate a high level of consistency and reliability in the results obtained in this study.

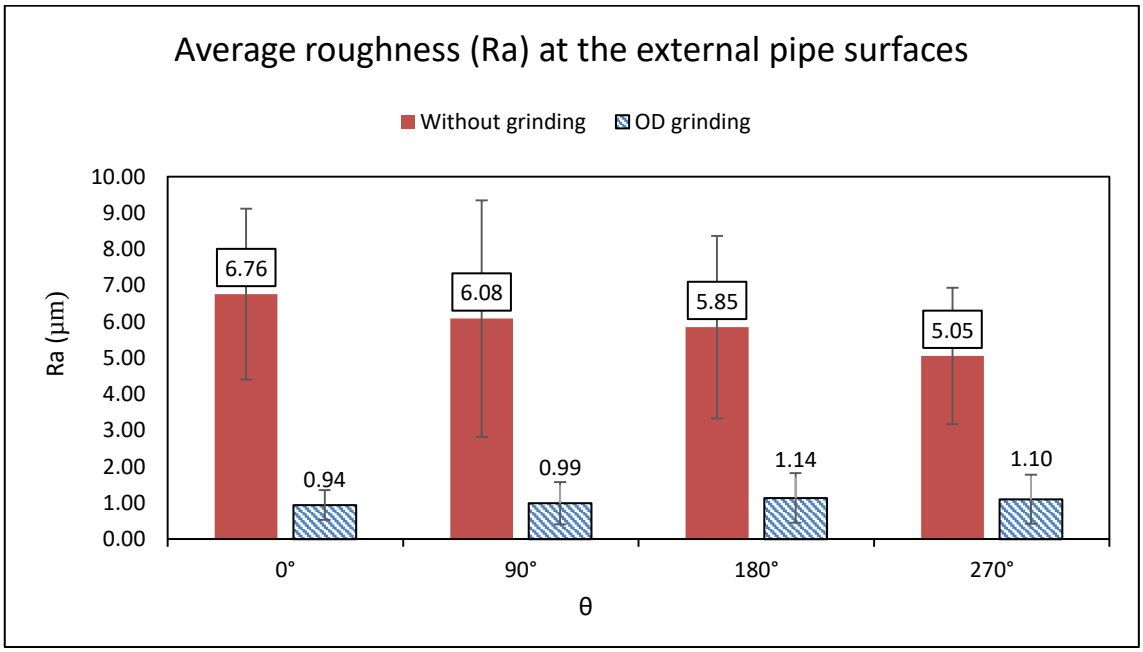

Figure 5.8 – Results of average roughness measured in the external surface in four positions separated by 90° in the area with and without grinding.

5.4 Fatigue properties

In this section, it will be presented the full-scale fatigue test results and the failure location of each specimen (with and without grinding).

Table 5.3 displays the stress range and pressure applied to each specimen, along with the minimum number of cycles required by the BS7608 standard [35] to validate Class DNV-RP-C203 Class B1 Design in Air. It also shows the number of cycles each specimen endured until failure, except for specimen R159-03, where the test was stopped at 32,000,000 cycles and then resumed under more severe conditions until its ultimate failure. It is worth noting that all unrepaired specimens achieved a higher number of cycles than the requirement stated in BS7608 [35] for class B1, with the exception of specimen R159-01, which endured 1,203,328 cycles, falling at a lower number of cycles than the standard requirement. Accordingly, the current results demonstrate a high level of durability and resilience in the unground seamless pipes.

Table 5.3 also presents the failure location of each unrepaired specimen. Three specimens (R159-01, R159-02 and R159-06) failed within 200 mm from the centre line (middle of the specimen length), two specimens (R159-03 and R150-04) failed from 250 mm to 500 mm of the centre line on side A, and only one specimen (R159-05) failed from 750 mm to 1100 mm of the centre line on side A.

Table 5.3 – Full scale fatigue test results on specimens without grinding. (C/L corresponds to center line)

Specimen	**p_i [MPa]**	**Δσ [MPa]**	**N (Number of cycles)**		**Failure location**
			BS7608 (class B1)	**Actual**	
R159-03	51,0	200	2.800.230	32.000.000	Test halted
	61,2	240		3.402.000	A side approx. 500 mm from C/L
R159-04	51,0	200		12.437.591	A side approx. 370 mm from C/L
R159-06	51,0	200		4.200.000	A side approx. 180 mm from C/L
R159-01	61,2	240	1.350.420	1.203.328	A side approx. 100 mm from C/L
R159-02	61,2	240		1.560.000	B side approx. 180 mm from C/L
R159-05	61,2	240		2.131.000	A side approx. 820 mm from C/L

Based on the test data, excluding R159-03 due to the test being halted, it can be confidently stated that the selection of DNV-RP-C203 B1 Design in Air class is valid according to BS7608 [35] considering the following constraints due to the statistical analysis associated with the number of pipes (n) tested in each condition:

- For $\Delta\sigma$ = 200 MPa, n = 2 leads to 4.293 factor i.e., S-N curve validity considering an interval of confidence of 99%;
- For $\Delta\sigma$ = 240 MPa, n = 3 leads to 1.874 factor i.e., S-N curve validity considering an interval of confidence of 95%;
- For a mean $\Delta\sigma$ value of 220 MPa, n = 5 leads to 4.555 factor i.e., S-N curve validity considering an interval of confidence of 95%.

According to Miner's rule associated with B1 parameters, the cumulated numbers of cycles at 200 MPa for R159-03 can be estimated to be N = 39,054,387.

In Table 5.4, it is presented the stress range and pressure (in ascending order) applied in each specimen. It also shows the minimum number of cycles required to validate BS7608 [35] to validate DNV-RP-C203 Class D Design in Air (corresponding to pipes with circumferential butt weld made from both sides), as well as the actual number of cycles of each specimen until pipe failure. This classification was confidently based on the available curve made with the actual number of cycles that are most similar to this class. This approach has been shown to have sufficient validity, with a confidence rate of over 95%.

- For $\Delta\sigma$ = 180 MPa, n = 2 leads to 2.537 factor i.e., S-N curve validity over 99%;
- For $\Delta\sigma$ = 200 MPa, n = 2 leads to 2.628 factor i.e., S-N curve validity over 99%;
- For $\Delta\sigma$ = 240 MPa, n = 2 leads to 2.139 factor i.e., S-N curve validity over 97.5%;
- For a mean $\Delta\sigma$ value of ~206.67 MPa, n = 6 leads to 4.229 factor i.e., S-N curve validity over 99%.

Table 5.4 - Full scale fatigue test results on specimens with grinding on ID. (C/L corresponds to center line)

Specimen	p_i [MPa]	Δσ [MPa]	N (Number of cycles)		Failure location
			BS7608 (Class D)	Actual	
R159-11	45.9	180	856,044	1,510,770	B side approx. 400 mm from C/L
R159-12	45.9	180		1,360,000	B side approx. 90 mm from C/L
R159-09	51.0	200	624,056	1,253,833	Center Line
R159-10	51.0	200		901,582	B side approx. 440 mm from C/L
R159-07	61.2	240	361,144	464,868	A side approx. 430 mm from C/L
R159-08	61.2	240		598,975	B side approx. 330 mm from C/L

It is evident that as the stress range increases in the test, the number of cycles required by BS7608 [35] to validate DNV-RP-C203 Class D Design in air decreases. This trend is also observed in the actual number of cycles that each specimen with internal grinding supported until failure. Moreover, all specimens with internal grinding achieved a higher number of cycles compared to the requirement of DNV-RP-C203 Class D.

The failure location of each specimen with internal griding is also presented in Table 5.4. It is possible to notice that most specimens (R159-07, R159-08, R159-10, and R159-11) fractured between 250 mm and 500 mm from the center line on the B side, except for R159-07, which fractured on the A side. Only one specimen (R159-09) fractured on the center line, and one specimen (R159-12) fractured within 200 mm from the center line on the B side.

Two seamless pipes with external grinding were subjected to full-scale fatigue testing with a stress range of 200 MPa and an internal pressure of 51 MPa. Table 5.5 shows the number of cycles each specimen supported. These results are for informational purposes only, as two tests are insufficient to draw statistical conclusions. However, the initial results suggest that the pipes fulfil the requirements for application demanding the DNV-RP-C203 Class C Design in Air (which corresponds to pipes with automatic longitudinal seam welds) based on BS7608 as for $\Delta\sigma = 200$ MPa, $n = 2$ leads to 4.390 factor i.e., S-N curve validity over 99%.

Table 5.5 - Full scale fatigue test results on specimens with external grinding. (C/L corresponds to center line)

Specimen	p_i [MPa]	Δσ [MPa]	N (Number of cycles)		Failure location
			BS7608 (Class C)	Actual	
R159-13	51.0	200	2,096,757	2,251,000	B side approx. 330 mm from C/L
R159-14	51.0	200		8,000,000	B side approx. 820 mm from C/L

The results in Table 5.5 revealed that when considering DNV-RP-C203 Class C Design in Air, all specimens with external grinding achieved a higher number of cycles compared to the DNV-RP-C203 requirement for Class C Design. Both specimens failed on the B side, but in different locations. R159-13 failed 330 mm from the centre line, while R159-14 fractured 820 mm from the centre line.

5.5 Analysis in fractured specimens

This section presents the analysis conducted on the seamless pipes after the full-scale fatigue test. The examinations include ultrasonic inspection to identify the location of failure relative to the repaired area, internal surface roughness measurements in the region with and without grinding, magnetic particle inspection (MPI) to identify fatigue cracks on the pipe surface, macroscopic and microscopic analysis.

Following the fatigue tests, ultrasonic inspections were conducted to accurately determine the location of the failure on the pipe surface profile, as shown in Figures 5.9 and 5.10 for specimens with internal and external grinding, respectively. The lines (orange or purple) in each figure represent the average diameter in each pipe section, whereas the dotted lines denote the minimum and maximum diameters in the same locations. The planes represented by the dotted vertical red line correspond to the positions of the strain gauges 1-16, already shown in Figure 4.7. The location of failure is indicated by the vertical line coloured in blue.

In Figure 5.9, it is evident that all pipes with internal grinding failed within the repaired area, specifically where the grinding began, except for specimen R159-10, which failed almost in the middle of the grinding area. The same behaviour can be observed in pipes

with external grinding shown in Figure 5.10 as both specimens failed within the repaired area where the grinding operation was initiated.

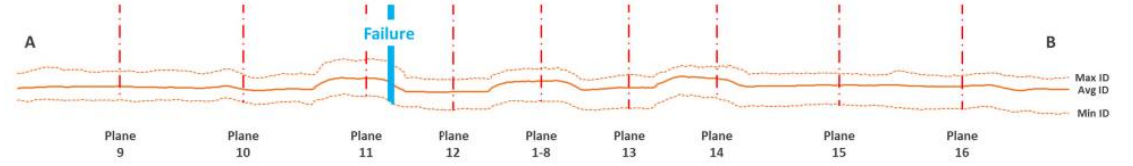

(a)

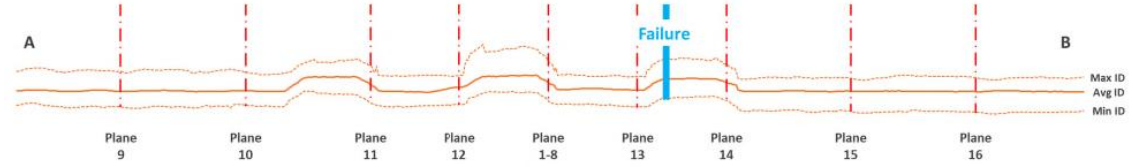

(b)

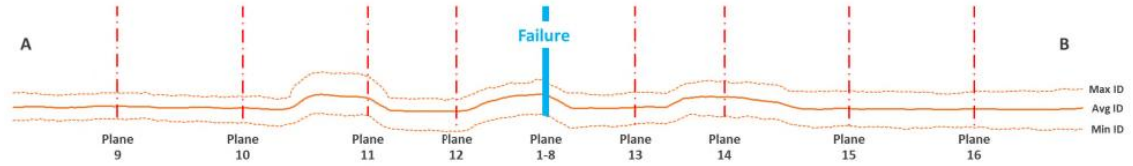

(c)

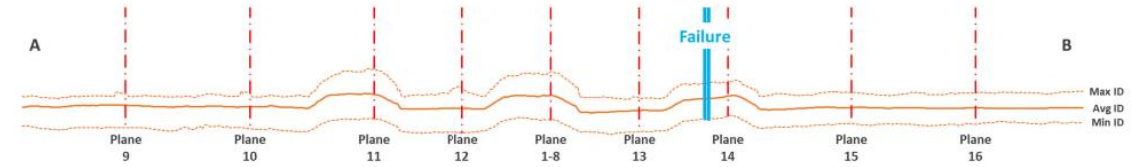

(d)

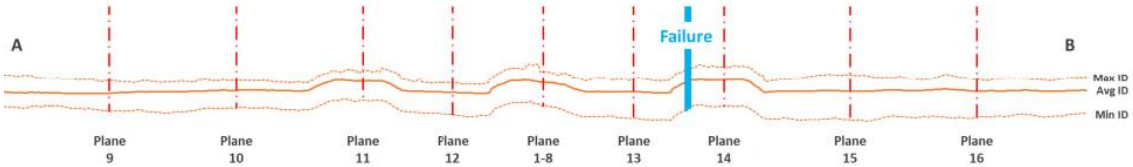

(e)

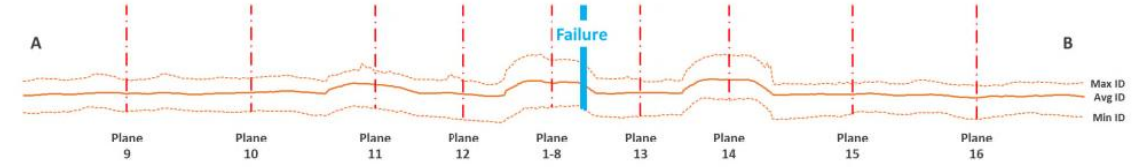

(f)

Figure 5.9 – Pipe failure location after the full-scale fatigue test in specimens with internal grinding: (a) R159-07; (b) R159-08; (c) R159-09; (d) R159-10; (e) R159-11; (f) R159-12

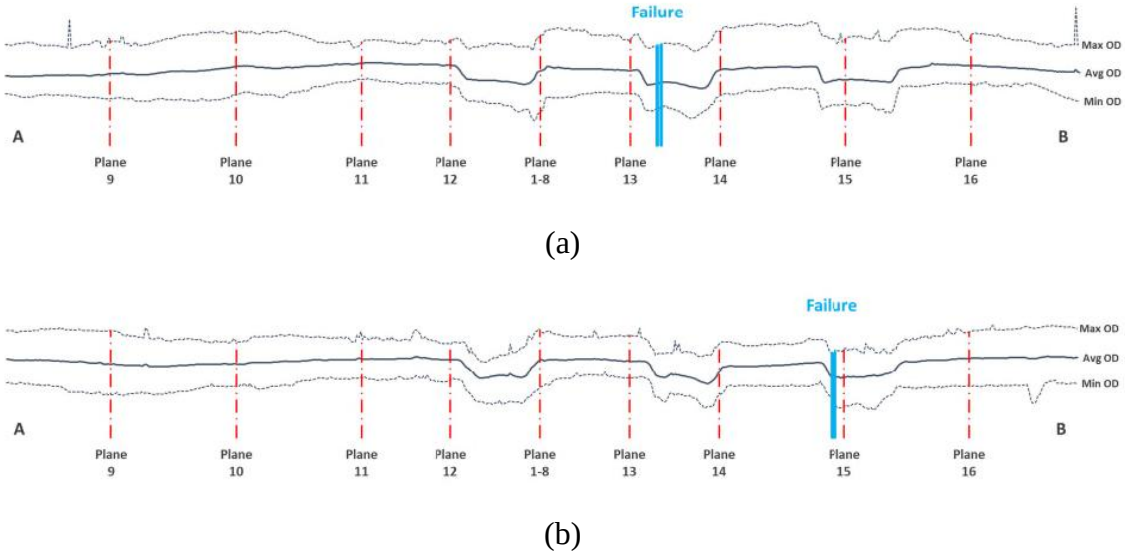

Figure 5.10 - Pipe failure location after the full-scale fatigue test in specimens with external grinding: (a) R159-13; (b) R159-14

The roughness parameter (Ra) at the internal surfaces of the seamless pipes with internal grinding (R159-07 to R159-12) was measured in both the ground and unground regions after full-scale fatigue testing. Figure 5.11 displays the average values (Ra) for these regions. It is evident that the roughness of the internal surface increased with the grinding process. The region without grinding had an average roughness of 3.44 µm, while the repaired region had an average roughness of 9.41 µm. Nevertheless, statistical analysis shows that both regions had similar standard deviations, indicating that there was little variability in roughness between each tested specimen.

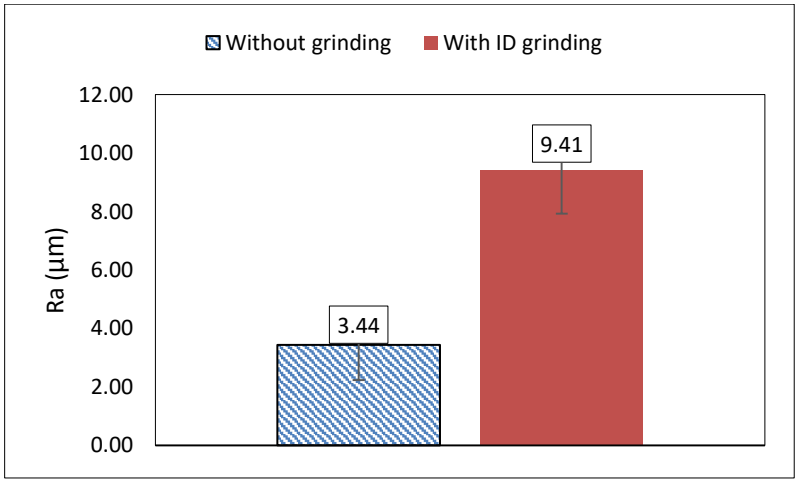

Figure 5.11 – Average roughness (Ra) in the internal surfaces of a seamless pipe after internal grinding.

Magnetic particle inspection (MPI) was conducted to detect fatigue cracks on the pipe surface, as shown in Figure 5.12 for representative specimens of seamless pipes after fatigue testing (specimens R159-04, R159-09 and R159-13). For each specimen, first it was presented the external surface and, second, the internal surface inspection. The red arrows point to the identified indications.

In specimen R159-04 (without grinding), it was noticed an indication with 13 mm length in the external surface and another of 46 mm length in the internal surface. In specimens R159-09 (with internal grinding), it was seen an indication with 17 mm in the external surface and two indications in the internal surface with 69 mm and 27 mm length. In specimen R159-13 (with external grinding), there was indication only on the external surface that had a length of 57 mm. Therefore, it appears that the largest indications typically appear on the internal surface, except for specimens that underwent external grinding, where the largest indication appeared on the external surface. Nevertheless, all specimens exhibited transverse indications.

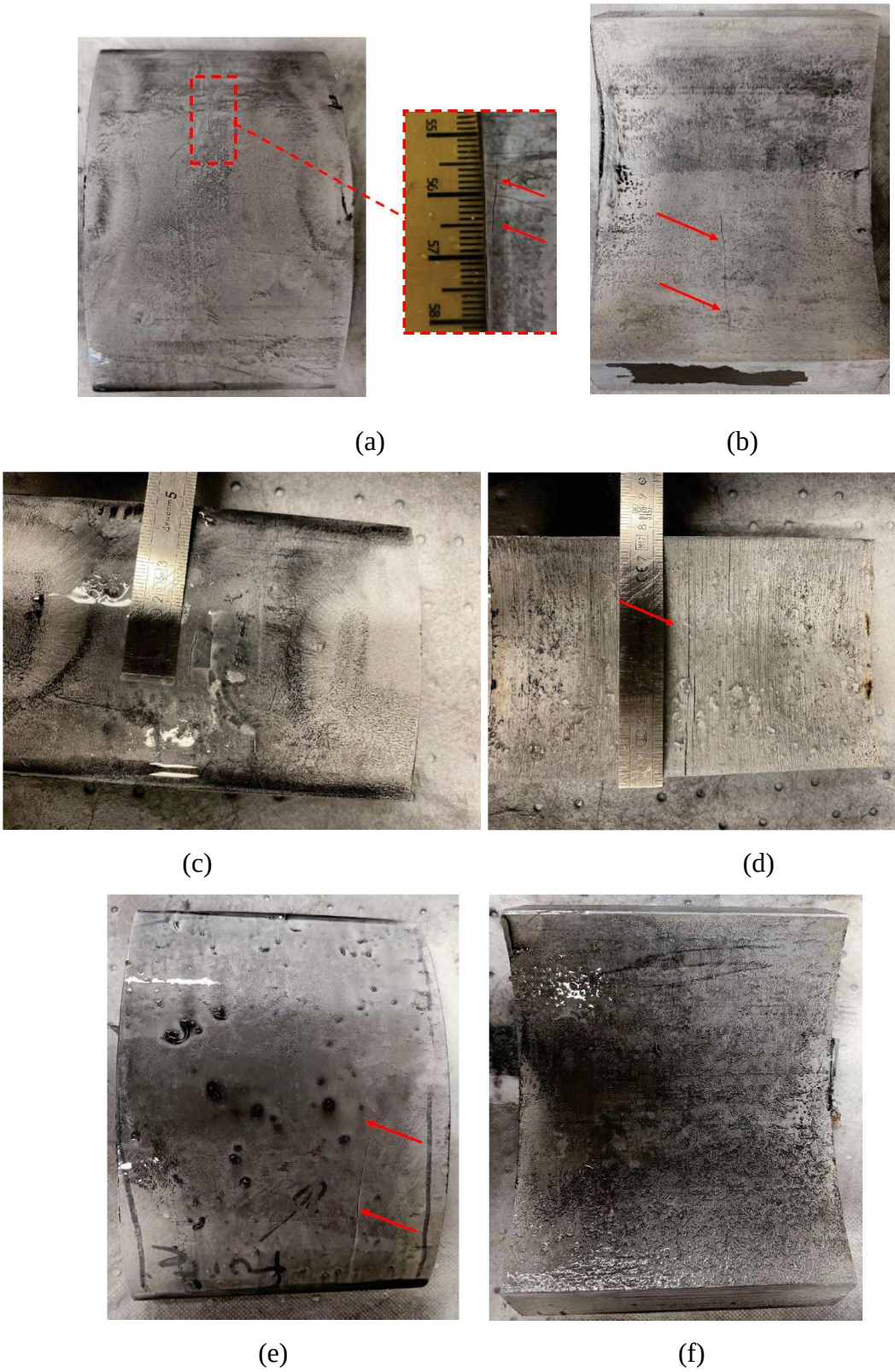

Figure 5.12 –MPI in longitudinal direction, first in external surface and second, in internal surface. (a) and (b) Specimen R159-04 (without grinding); (c) and (d) Specimen R159-09 (with internal grinding); (e) and (f) Specimen R159-13 (with external grinding).

Each sample was then examined at the vicinity of the longest indication of MPI to produce a macrograph of the fracture surface. Figure 5.13 shows the macrographs of typical specimens for each surface condition: R159-04 (without grinding), R159-09 (with internal grinding), and R159-13 (with external grinding). The blue arrows indicate the location where the cracks originated.

The evaluation of macrographs revealed that the cracks originated from the internal surfaces and propagated towards the external surfaces in the majority of the seamless pipes, except for the unground specimen R159-03 (which had the longest fatigue life) and the specimens which external grinding, where the cracks started from the external surfaces and propagated towards the internal surfaces. Furthermore, all specimens exhibited the presence of typical lunulas.

Evaluation with SEM was made in all specimens in at least two regions. The SEM analyses revealed the presence of fatigue striations in all specimens that were not highly oxidized. These fatigue striations are pointed by blue arrows in Figure 5.14 for the material which underwent internal (R159-09) and external (R159-13) grinding. It should be noted that the SEM images in Figure 5.14 were acquired within the red dotted area marked in Figure 5.13.

Therefore, with the metallography evaluation, one can conclude that all fractures were confirmed to be due to fatigue crack propagation.

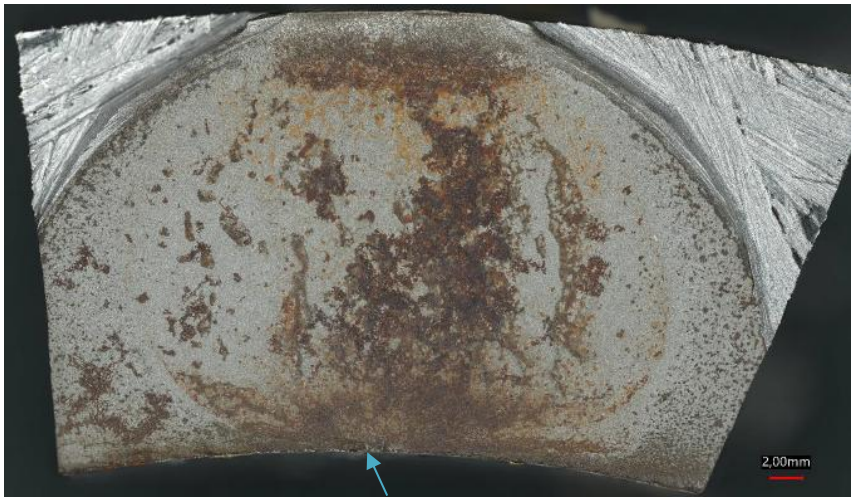

(a)

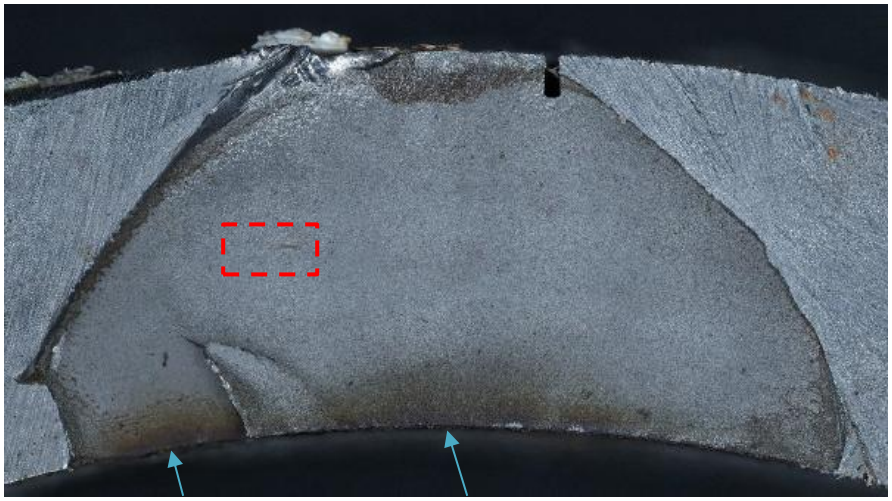

(b)

(c)

Figure 5.13 – Macrography in the fracture surface of specimen (a) R159-04 (without grinding); (b) R159-09 (with internal grinding) and (c) R159-13 (with external grinding). Presence of lunula. Arrows point to where the crack started

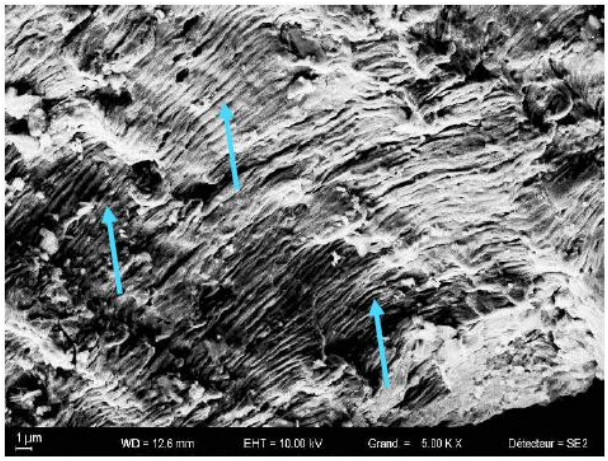

(a)

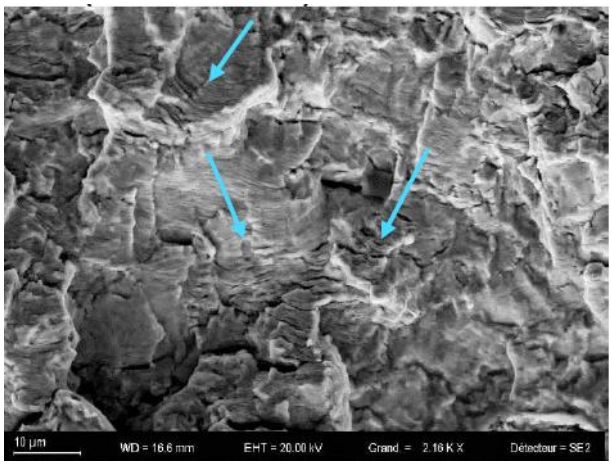

(b)

Figure 5.14 – SEM analysis of (a) specimen R159-09 and (b) specimen R159-13 in the dotted are of macrography inspection. Blue arrows points to fatigue striations.

6 DISCUSSION

The current investigation mainly aimed to evaluate the effect of grinding operations on the surface of X65Q PSL2 seamless pipes on their fatigue life. The results revealed that the fatigue endurance of the material tested under different nominal stress amplitudes significantly decreased in the ground pipes when compared with the unrepaired material. As follows from examinations of the fatigue results according to the API 5L standard [5], the seamless pipes achieved the DNV-RP-C203 Class B1 - Design in Air requirements whereas they reached a fatigue performance compatible with DNV-RP-C203 Class C and D - Design in Air after grinding. To elucidate the reasons underlying the encountered material behaviour the following hypotheses are carefully evaluated:

a) Differences in the microstructures of the pipes next to the ground areas.
b) Modifications in the roughness of the pipe surfaces provoking local stress concentrations after grinding.
c) Increase in local stresses due to the imprint of superficial notches in the ground pipes.

For this study, high-strength steels compatible with the line pipe application were designed to permit the achievement of high fatigue endurance under longitudinal stresses. Accordingly, the seamless pipes should display high toughness and reasonable homogeneity. These requirements were successfully attained as confirmed through the mechanical properties recorded during tensile and impact testing together with the hardness measurements.

The API 5L standard [5] requires a yield strength of 450-570 MPa for this grade. All tested pipes achieved a yield strength greater than 480 MPa with a maximum variation of 26 MPa along the pipe length and circumference. The material also demonstrated high toughness at -40°C, with an average absorbed energy consistently greater than 397 J and a shear fracture area of 100%. In terms of hardness, API 5L requires a maximum individual hardness of 250 HV10 for sour service materials, which the material met as the hardness values did not exceed 237 HV10. In addition, there is a maximum variation

of 21 HV10 in the average microhardness along the pipe thicknesses and circumferential positions (0° and 180°). Therefore, there is no evidence of a significant difference between the static mechanical properties of the unrepaired and ground tubes such that it is reasonable to deny the hypothesis that microstructural changes yielded the decrease of fatigue endurance after grinding. Considering those results of mechanical properties, it was considered that there was no evidence of a significant difference between the tubes and the hypothesis of a microstructure change between the pipes could be discarded.

Two different types of grinding operation were performed on the pipe surface, resulting in a change in the pipe roughness for each operation. The internal surface was subjected to an automatic dry grinding with a lance in which it was possible to measure the roughness in this surface only after the fatigue test. To ensure accurate surface quality analysis, the surface was cleaned with a brush to remove rust that could affect the results. Despite this operation, the roughness scans performed in the internal surfaces of the pipes tested in fatigue revealed an increase in the average roughness (R_a) from ~3.4 µm, as measured in the unrepaired areas, to ~9.4 µm in the ground areas.

The external surfaces of a second set of pipes were subjected to manual grinding. The R_a values in the unrepaired regions of these pipes ranged from ~5.0 to 6.8 µm, whereas the average roughness sugnificantly diminished to ~1 µm in the ground external surfaces.

Itoga et al. (2003) [37] confirmed through SEM examination that cracks initiate at the bottom of scratch marks. This indicates that surface roughness acts as a small notch, which can enhance stress concentration at the bottom, leading to premature crack initiation and decreased fatigue strength with increasing surface roughness. As surface roughness increases, stress concentration also increases, resulting in cracks always initiating at scratch marks on the specimen surface.

Nevertheless, even though the Ra values increased for the internal surfaces of the tubes subjected to automatic grinding it is likely that the modification on surface roughness was not the primary factor in reducing the fatigue life of the material. This follows from the reduction in the average roughness of the external surfaces of the pipes subjected to

manual grinding as they showed a decrease in the Ra values, but their fatigue endurances were still reduced.

Related to the grinding operation performed, Kopac and Krajnik (2006) [38] define grinding as a complex abrasive cutting process that is related to machining with geometrically unspecified cutting edges. The grinding interface involves the removal of material through contact between a grinding wheel with a randomly structured topography and the workpiece. Each grain removes a chip from the surface of the workpiece material and generates a surface finish. The process of grinding refers to the removal of material by individual grains whose cutting edge is bounded by force and path. The conditions of interface friction, material flow characteristics, and cutting speed significantly influence chip formation.

In conclusion, further studies are required to improve the knowledge of the cause and effect of pipe roughness in the fatigue life of X65Q seamless pipes. Additional studies are also required to assess the possibility of improving the pipe roughness after automatic dry grinding with a lance on the internal surface, as this is a very complex operation where more than one action could affect the pipe roughness and, as a consequence, the fatigue resistance.

This study also aimed to examine the fatigue endurance of X65Q seamless tubes in order to classify this material according to the guidelines provided by the Standard BS 7608 [35]. All pipes without grinding were classified as DNV-RP-C203 Class B1 Design in Air, which corresponds to hollow sections fabricated without welding. Regarding crack initiation and propagation, it has been observed that, in all unrepaired pipes, apart from specimen R159-03, the cracks originated from the internal surfaces and gradually propagated towards their external surfaces as evident from the typical fatigue striations shown in the SEM images. Zhao et al. (2016) [39] investigated the fatigue properties of X80 pipeline using small specimens and also observed that the fatigue crack initiation of the full thickness specimens occurred at the surface of the rolled steel plates and the fatigue crack grew inward until the fracture formed.

Figure 6.1 displays the relationship between the stress range and the number of fatigue cycles, in which the unground specimens are green triangles, specimens with integral grinding are red circles and specimens with external grinding are yellow rhombuses. It readily seen that grinding leads to a sizable reduction in the fatigue endurance of the steel pipes, as almost all the unrepaired specimens achieved a higher fatigue life than its ground counterparts at comparable testing conditions. It also demonstrated that the pipes repaired by internal grinding displayed a comparatively lower fatigue endurance.

Consequently, as demonstrated in the Results, they were classified as DNV-RP-C203 Class D Design in Air. On the other hand, the pipes repaired by external grinding were classified as DNV-RP-C203 Class C Design in Air due to its somewhat superior fatigue resistance. It is important to note that cracking initiated at the ground areas of the X65QS seamless tubes, and this led to the onset of cracks distanced from the centerlines of the tubes, in which it is expected the presence of higher stresses during fatigue testing of ideal specimens. Furthermore, the metallographic analysis confirmed the presence of fatigue striations, indicating that the fracture was caused by fatigue.

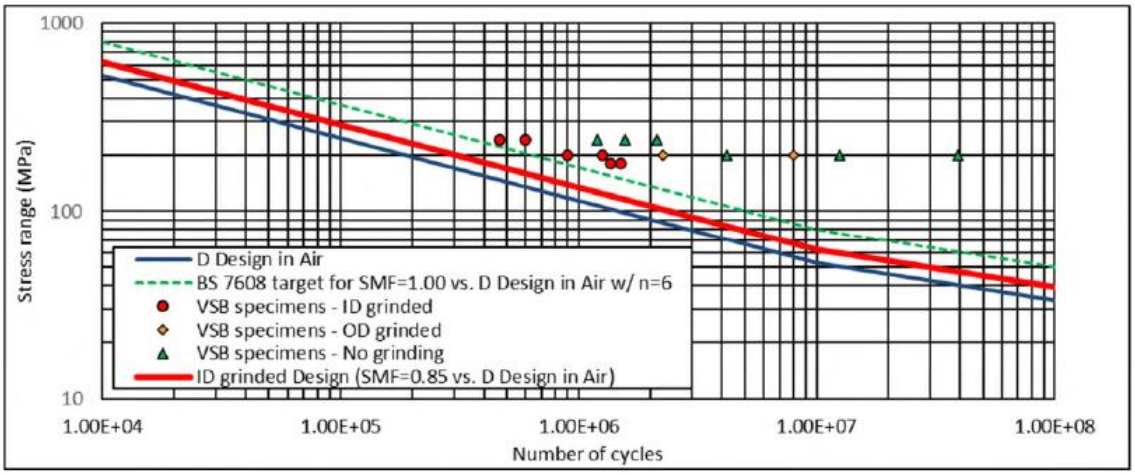

Figure 6.1 – Relationship between the stress range and the number of fatigue cycles for the seamless pipes tested in this study. The S-N curves are also plotted for comparison purposes considering the requirements of the S-N class DNV D Design in Air with different SMF.

According to DNV-RP-C203 [31], to validate the use of a design S-N class based on a limited number of new fatigue tests, it is necessary to derive from statistic the so-called Stress Modification Factor (SMF) which considers the presence of geometrical discontinuities leading to stress concentrators in the tested specimens. As follows from

Figure 6.1, an increase in the SMF value leads to the displacement of the S-N curves to the right-hand side which follows from the assumed presence of defects resulting in higher stress gradients than in the standard curve (blue line) for the chosen S-N class. It is readily noted that all datum points lie above the red solid line corresponding to the minimum performance targeted for SMF = 0.85 vs DNV D Design in Air, but they are dangerously close to the dashed green line in which SMF = 1.00 vs DNV D Design in Air. Accordingly, it is reasonable to consider that the ground pipes can be used for applications consonant with the S-N class D Desing in Air considering an SMF value of 0.85.

It follows from the results recorded by ultrasonic inspection, the main reason underlying the inferior fatigue life of steel pipes repaired by internal grinding is likely associated with the local reduction in the wall thickness of the pipes. It gives rise to geometrical discontinuities (small steps) at the internal surfaces of the pipes as apparent in Figures 5.5 and 5.6.

It should be however noted that when the external surfaces of the pipes underwent grinding, the procedure was carried out manually. This apparently led to more stable processing conditions and ultimately resulted in the removal of a lower volume of material and geometrical discontinuities with comparably lower dimensions. Therefore, it is possible that the main reason of the inferior fatigue life reduction of steel pipes repaired in the external grinding could be associated with the procedure of manual grinding, like the direction of grinding.

According to Standard BS 7608 [35], fatigue cracks typically initiate at surface irregularities, corners of cross sections, or holes and re-entrant corners in non-welded parts. Additionally, the presence of unspecified notches in a new product can have the same effect on the remaining fatigue life as a fatigue crack of the same size. Therefore, such notches can significantly shorten the fatigue life of the product by eliminating the period of early crack growth. Also, notches oriented normal to the direction of fluctuating stress and located at the surface of the product are even more detrimental. The seamless steel pipes repaired by grinding fulfill the aforementioned features which reasonably

explain their inferior fatigue endurance. The same effect has been reported in recent studies, including in experiments carried out using small-scale specimens [40, 41].

The current results highlight the importance of conducting full-scale fatigue tests to certify that the product fulfills the requirements for applications in hazardous conditions. The effect of grinding in the fatigue life would not be identified if small-scale fatigue tests were performed. Further studies are paramount to examine the effect of grinding conditions on the fatigue endurance of seamless pipes in order to diminish the detrimental effect associated with the development of geometrical discontinuities.

7 CONCLUSIONS (CONCLUSÕES)

7.1 English version

1. The effect of surface grinding on the fatigue life of X65Q PSL2 seamless pipes was examined through careful experiments including full-scale fatigue tests.

2. The fatigue endurance of the X65Q PSL2 tubes significantly decreased because of grinding, and this was more prominent for the pipes subjected to automatic grinding at their internal surfaces. The original pipes complied with DNV-RP-C203 Class B1 - Design in Air, whereas the tubes ground at either the external or internal surfaces achieved a fatigue life compatible with DNV-RP-C203 Class C and D, respectively.

3. There was no evidence that microstructural changes yielded the decrease of fatigue endurance after grinding as the hardness values and the tensile properties of all pipes are within the expected ranges, without marked differences that could justify the distinct fatigue behaviors.

4. Although grinding led to an increase in the surface roughness of the pipes subjected to internal grinding, this did not appear to stand as the primary factor in reducing their fatigue life. This follows from the decrease in the average roughness from ~5.0-6.8 to ~0.9-1.1 μm for pipes subjected to the external grinding concomitantly with a decrease in their fatigue endurance.

5. The decrease in fatigue life for the steel pipes repaired by grinding is likely associated with the local reduction in the wall thickness of the pipes at the vicinity of the repaired areas. As confirmed through ultrasonic inspection, this gives rise to small notches in the ground material which are more prominent after internal grinding, the same material condition that lower fatigue endurances. These notches are oriented normal to the direction of fluctuating stress and may act as stress concentrators, shortening the fatigue life of the pipes by eliminating the period of early crack growth.

7.2 Portuguese version

1. O efeito da retificação superficial na vida útil à fadiga de tubos sem costura X65Q PSL2 foi examinado por meio de experimentos cuidadosos, incluindo testes de fadiga em escala real.

2. A resistência à fadiga dos tubos X65Q PSL2 diminuiu significativamente devido à operação de retificação, e isso foi mais pronunciado para os tubos submetidos ao procedimento automático nas superfícies internas. Os tubos originais estavam em conformidade com o DNV-RP-C203 Classe B1 - Design em Ar, enquanto os tubos reparados nas superfícies externas ou internas alcançaram uma vida útil à fadiga compatível com DNV-RP-C203 Classe C e D, respectivamente.

3. Não houve evidências de que mudanças microestruturais causaram a diminuição da resistência à fadiga após a retificação, uma vez que os valores de dureza e as propriedades de tração de todos os tubos estão dentro das faixas esperadas, sem diferenças marcadas que pudessem justificar os diferentes comportamentos de fadiga.

4. Embora a retificação tenha levado a um aumento na rugosidade superficial dos tubos submetidos ao reparo interno, isso não parece ser o principal fator na redução da vida útil à fadiga. Isso se segue da diminuição da rugosidade média de ~5,0-6,8 para ~0,9-1,1 µm para tubos submetidos à retificação externa, concomitantemente com a diminuição de sua vida em fadiga.

5. A diminuição da vida útil à fadiga para os tubos de aço retificados está provavelmente associada à redução local na espessura da parede dos tubos nas proximidades das áreas reparadas. Conforme confirmado por inspeção ultrassônica, isso dá origem a pequenos rebaixos no material retificado, que são mais proeminentes após o reparo interno, a mesma condição de material que reduz a resistência à fadiga. Esses rebaixos estão orientados normalmente à direção do estresse flutuante e podem atuar como concentradores de tensão, encurtando a vida útil à fadiga dos tubos ao eliminar o período de crescimento precoce de trincas.

8 SUGGESTION FOR FUTURE WORKS

- As demonstrated in this study, the transition area (tapering) between the ground and unground regions had a significant impact on the fatigue life of X65Q PSL2 seamless pipes. Therefore, future research should focus on evaluating this transition area and developing strategies to mitigate its detrimental effects on the material's fatigue life.

  Evaluate the effects of the finishing repair (including the impact of the direction, whether longitudinal or transverse, and roughness) on the external and internal surface of the material’s fatigue resistance.

REFERENCES

[1] L.B. Godefroid, B.M. Sena, V.B. da Trindade Filho, Evaluation of Microstructure and Mechanical Properties of Seamless Steel Pipes API 5L Type Obtained by Different Processes of Heat Treatments, Materials Research 20 (2017) 514–522. https://doi.org/10.1590/1980-5373-mr-2016-0545.

[2] L.L.S. Mathias, D.F.B. Sarzosa, C. Ruggieri, Effects of specimen geometry and loading mode on crack growth resistance curves of a high-strength pipeline girth weld, International Journal of Pressure Vessels and Piping 111–112 (2013) 106–119. https://doi.org/10.1016/j.ijpvp.2013.06.003.

[3] S.K. Sharma, S. Maheshwari, A review on welding of high strength oil and gas pipeline steels, J Nat Gas Sci Eng 38 (2017) 203–217. https://doi.org/10.1016/j.jngse.2016.12.039.

[4] M.J. Kaiser, Offshore Overview, in: The Offshore Pipeline Construction Industry, Elsevier, 2020: pp. 3–38. https://doi.org/10.1016/b978-0-12-820288-3.00001-9.

[5] American Petroleum Institute, API SPECIFICATION 5L, 46th ed., 2018.

[6] R. Singh, Classification of Steels, in: Applied Welding Engineering, Elsevier, 2016: pp. 57–64. https://doi.org/10.1016/b978-0-12-804176-5.00006-2.

[7] J.C. Villalobos, A. Del-Pozo, B. Campillo, J. Mayen, S. Serna, Microalloyed steels through history until 2018: Review of chemical composition, processing and hydrogen service, Metals (Basel) 8 (2018). https://doi.org/10.3390/met8050351.

[8] D.-I. Hans-Georg Hillenbrand, D.-I. Michael Gras, D.-I. Christoph Kalwa, DEVELOPMENT AND PRODUCTION OF HIGH STRENGTH PIPELINE STEELS, n.d.

[9] R. Langbauer, G. Nunner, T. Zmek, J. Klarner, R. Prieler, C. Hochenauer, Investigation of the temperature distribution in seamless low-alloy steel pipes during the hot rolling process, Advances in Industrial and

Manufacturing Engineering 2 (2021). https://doi.org/10.1016/j.aime.2021.100038.

[10] Z. Ling, J. Fang, Y. Zhou, Z. Yuan, Influence of Quenching On-line on Properties of X70 Steel for Sour Service Seamless Pipe, in: Energy Procedia, Elsevier Ltd, 2012: pp. 444–450. https://doi.org/10.1016/j.egypro.2012.01.072.

[11] Q. Wu, S. He, P. Hu, Y. Liu, Z. Zhang, C. Fan, R. Fan, N. Zhong, Effect of finish rolling temperature on microstructure and mechanical properties of X80 pipeline steel by on-line quenching, Materials Science and Engineering A 862 (2023). https://doi.org/10.1016/j.msea.2022.144496.

[12] L.N. Pussegoda A', R. Barbosa, S. Yue, J.J. Jonas, P.J. Hunt, Laboratory simulation of seamless-tube rolling, 1991.

[13] H. Colpaert, Metalografia dos produtos siderúrgicos comuns, 2008.

[14] W.D. CALLISTER, Ciência e Engenharia de Materiais - Uma Introdução, 2018.

[15] J. Niu, L.H. Qi, Y.L. Liu, L. Ma, Y.R. Feng, J.X. Zhang, Tempering microstructure and mechanical properties of pipeline steel X80, Transactions of Nonferrous Metals Society of China (English Edition) 19 (2009). https://doi.org/10.1016/S1003-6326(10)60111-2.

[16] G.P. Drumond, I.P. Pasqualino, B.C. Pinheiro, S.F. Estefen, Pipelines, risers and umbilicals failures: A literature review, Ocean Engineering 148 (2018) 412–425. https://doi.org/10.1016/j.oceaneng.2017.11.035.

[17] M. Kristoffersen, M. Langseth, T. Børvik, Combined three-point bending and axial tension of pressurised and unpressurised X65 offshore steel pipes – Experiments and simulations, Marine Structures 61 (2018) 560–577. https://doi.org/10.1016/j.marstruc.2018.06.005.

[18] Q. Bai, Y. BAI, Subsea Pipeline Design, Analysis, and Installation, Elsevier, 2014. https://doi.org/10.1016/C2010-0-67706-6.

[19] Fairtex, Supply of Subsea Umbilicals, Risers and Flowlines (SURF), (n.d.). https://fairtex.com.ng/procurement.of/subsea-umbilicals-risers-and-flowlines-surf/129/ (accessed February 21, 2023).

[20] A. Manes, R. Porcaro, H. Ilstad, E. Levold, M. Langseth, T. Børvik, The behaviour of an offshore steel pipeline material subjected to bending and stretching, Ships and Offshore Structures 7 (2012) 371–387. https://doi.org/10.1080/17445302.2011.606699.

[21] L. Poberezhnyi, P. Maruschak, O. Prentkovskis, I. Danyliuk, T. Pyrig, J. Brezinová, Fatigue and failure of steel of offshore gas pipeline after the laying operation, Archives of Civil and Mechanical Engineering 16 (2016) 524–536. https://doi.org/10.1016/j.acme.2016.03.003.

[22] P. Xie, Q. Yue, A.C. Palmer, Cyclic plastic deformation of overbend pipe during deepwater S-lay operation, Marine Structures 34 (2013) 74–87. https://doi.org/10.1016/j.marstruc.2013.08.003.

[23] B. Senthil, R.P. Selvam, Dynamic analysis of a J-lay pipeline, in: Procedia Eng, Elsevier Ltd, 2015: pp. 730–737. https://doi.org/10.1016/j.proeng.2015.08.358.

[24] N. Nourpanah, F. Taheri, Development of a reference strain approach for assessment of fracture response of reeled pipelines, Eng Fract Mech 77 (2010) 2337–2353. https://doi.org/10.1016/j.engfracmech.2010.04.030.

[25] P. Jia, H. Jing, L. Xu, Y. Han, L. Zhao, A modified reference strain method for engineering critical assessment of reeled pipelines, Int J Mech Sci 105 (2016) 23–31. https://doi.org/10.1016/j.ijmecsci.2015.11.003.

[26] Y. Liu, S. Kyriakides, Effect of geometric and material discontinuities on the reeling of pipelines, Applied Ocean Research 65 (2017) 238–250. https://doi.org/10.1016/j.apor.2017.04.006.

[27] O. Fatoba, R. Akid, Low cycle fatigue behaviour of API 5L X65 pipeline steel at room temperature, in: Procedia Eng, Elsevier Ltd, 2014: pp. 279–286. https://doi.org/10.1016/j.proeng.2014.06.263.

[28] Canadian Association of Petroleum Producers (CAPP), Mitigation of Internal Corrosion in Sour Gas Pipeline Systems, Alberta, 2009.

[29] A. Olamide, A. Bennecer, S. Kaczmarczyk, Finite Element Analysis of Fatigue in Offshore Pipelines with Internal and External Circumferential Cracks, Applied Mechanics 1 (2020) 193–223. https://doi.org/10.3390/applmech1040013.

[30] C.R.A. Schneider, S.J. Maddox, BEST PRACTICE GUIDE ON STATISTICAL ANALYSIS OF FATIGUE DATA, The Welding Institute, 2003.

[31] DNV GL, RECOMMENDED PRACTICE DNV GL AS RP-C203: Fatigue design of offshore steel structures, 2014. www.dnvgl.com.

[32] Q. Bai, Y. Bai, Fatigue and Fracture, in: Subsea Pipeline Design, Analysis, and Installation, Elsevier, 2014: pp. 283–318. https://doi.org/10.1016/B978-0-12-386888-6.00012-2.

[33] DNV GL, RECOMMENDED PRACTICE DNV GL AS RP-C203: Fatigue design of offshore steel structures, 2014. www.dnvgl.com.

[34] O. Fatoba, R. Akid, Uniaxial cyclic elasto-plastic deformation and fatigue failure of API-5L X65 steel under various loading conditions, Theoretical and Applied Fracture Mechanics 94 (2018) 147–159. https://doi.org/10.1016/j.tafmec.2018.01.015.

[35] Guide to fatigue design and assessment of steel products, BSI Standards Publication Second (2014).

[36] API RECOMMENDED PRACTICE, System Configuration and Operation for Subsea Well Intervention Systems 17G1, 2021.

[37] H. Itoga, K. Tokaji, M. Nakajima, H.N. Ko, Effect of surface roughness on step-wise S-N characteristics in high strength steel, Int J Fatigue 25 (2003) 379–385. https://doi.org/10.1016/S0142-1123(02)00166-4.

[38] J. Kopac, P. Krajnik, High-performance grinding-A review, J Mater Process Technol 175 (2006) 278–284. https://doi.org/10.1016/j.jmatprotec.2005.04.010.

[39] Z. peng Zhao, G. ying Qiao, L. Tang, H. wei Zhu, B. Liao, F. ren Xiao, Fatigue properties of X80 pipeline steels with ferrite/bainite dual-phase microstructure, Materials Science and Engineering: A 657 (2016) 96–103. https://doi.org/10.1016/j.msea.2016.01.043.

[40] D. Liao, S.P. Zhu, J.A.F.O. Correia, A.M.P. De Jesus, F. Berto, Recent advances on notch effects in metal fatigue: A review, Fatigue Fract Eng Mater Struct 43 (2020) 637–659. https://doi.org/10.1111/ffe.13195.

[41] Z. Zhou, A. Andriyana, D. Guan, J. Chen, Evaluating the fatigue life of notched components based on the stress gradient model with variable support effects, Mater Des 239 (2024). https://doi.org/10.1016/j.matdes.2024.112793.